ACS OMEGA

http://pubs.acs.org/journal/acsodf

Article

Using Molecular Simulations for Elucidation of Thermodynamic Nonidealities in Adsorption of CO_2-Containing Mixtures in NaX Zeolite

Rajamani Krishna* and Jasper M. van Baten

Cite This: *ACS Omega* 2020, 5, 20535−20542

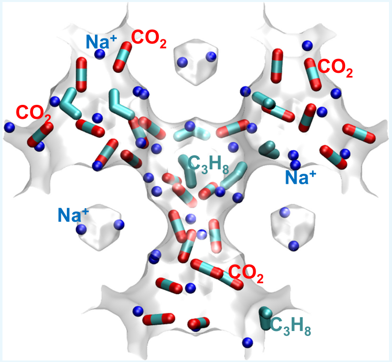

ABSTRACT: Cation-exchanged zeolites are of potential use in pressure swing adsorption (PSA) technologies for CO_2 capture applications. Published experimental data for CO_2/CH_4, CO_2/N_2, and CO_2/C_3H_8 mixture adsorption in NaX zeolite, also commonly referred to by its trade name 13X, have demonstrated that the ideal adsorbed solution theory (IAST) fails to provide adequately accurate estimates of mixture adsorption equilibrium. In particular, the IAST estimates of CO_2/CH_4 and CO_2/N_2 selectivities are significantly higher than those realized in experiments. For CO_2/C_3H_8 mixtures, the IAST fails to anticipate the selectivity reversal phenomena observed in experiments. In this article, configurational-bias Monte Carlo (CBMC) simulations are employed to provide confirmation of the observed thermodynamic nonidealities in adsorption of CO_2/CH_4, CO_2/N_2, and CO_2/C_3H_8 mixtures in NaX zeolite. The CBMC simulations provide valuable insights into the root cause of the failure of the IAST, whose applicability mandates a homogeneous distribution of adsorbates within the pore landscape. By sampling 10^5 equilibrated spatial locations of individual guest molecules within the cages of NaX zeolite, the radial distribution functions (RDFs) of each of the pairs of guest molecules are determined. Examination of the RDFs clearly reveals congregation effects, wherein the CO_2 guests occupy positions in close proximity to the Na^+ cations. The positioning of the partner molecules (CH_4, N_2, or C_3H_8) is further removed from the CO_2 guest molecules; consequently, the competition in mixture adsorption faced by the partner molecules is less severe than that anticipated by the IAST. The important message to emerge from this article is the need for quantification of thermodynamic nonideality effects in mixture adsorption.

1. INTRODUCTION

In current industrial practice, amine absorption technologies, which are energy intensive, are used for capture of CO_2 from a variety of gaseous mixtures. Potential reduction in the energy consumption is achievable using pressure swing adsorption (PSA) processes,[1−4] which are normally conducted in fixed-bed adsorbers.[4−7] A variety of microporous crystalline adsorbents such as zeolites and metal−organic frameworks (MOFs) can be employed in fixed-bed devices.[8−10] For postcombustion CO_2 capture, 13X zeolite is considered to be the benchmark adsorbent, with the ability to meet the U.S. Department of Energy (US-DOE) targets for CO_2 purity and recovery.[2] The commercially available 13X, a Na^+ cation-exchanged faujasite (FAU) zeolite with Si/Al ≈ 1.2, has wider applicability in natural gas purification[11,12] and alkane/alkene separations.[13]

For the design and development of PSA technologies, reliable procedures are required for the calculation of mixture adsorption equilibrium. For a microporous crystalline adsorbent with surface area A, we consider n-component adsorption equilibrium between a bulk fluid phase mixture with partial fugacities f_i and an adsorbed phase with component molar loadings q_i. The requirement of thermodynamic equilibrium demands equality of the chemical potentials of each component, μ_i, in the adsorbed phase and the bulk fluid phase

$$d\mu_i = RTd\ln f_i;\quad i = 1, 2, ..., n \tag{1}$$

The Gibbs adsorption equation[14−17] relates the spreading pressure π to the chemical potentials μ_i by the differential expression

$$A d\pi = \sum_{i=1}^{n} q_i d\mu_i \tag{2}$$

In the ideal adsorbed solution theory (IAST),[14] the partial fugacities f_i are related to the mole fractions x_i in the adsorbed phase mixture

Received: June 10, 2020
Accepted: July 24, 2020
Published: August 7, 2020

ACS Publications

https://dx.doi.org/10.1021/acsomega.0c02730

$$x_i = q_i/q_t; \quad q_t = q_1 + q_2 + \cdots + q_n; \quad i = 1, 2, ..., n \tag{3}$$

by introducing the sorption pressures, P_i^0, and invoking an analogy to Raoult's law for vapor−liquid equilibrium

$$f_i = x_i P_i^0; \quad i = 1, 2, ..., n \tag{4}$$

If $q_i^0(f)$ represents the *pure* component adsorption isotherms for each guest constituent in the mixture, the sorption pressures P_i^0 for each component in the mixture must satisfy the constraint

$$\frac{\pi A}{RT} = \int_0^{P_1^0} \frac{q_1^0(f)}{f} df = \int_0^{P_2^0} \frac{q_2^0(f)}{f} df = \int_0^{P_3^0} \frac{q_3^0(f)}{f} df = \cdots \tag{5}$$

An equation solver is required to determine the set of n values P_i^0. When P_i^0 are used as the upper limits in the definite integrals in eq 5, these result in the same value of the adsorption potential $\pi A/RT$, which serves as a practical proxy for the spreading pressure π. The adsorbed phase mole fractions x_i are then determined from

$$x_i = \frac{f_i}{P_i^0}; \quad i = 1, 2, ..., n \tag{6}$$

A number of experimental investigations[2,16−26] for adsorption of CO_2-containing binary mixtures in cation-exchanged zeolites demonstrate that the IAST does not provide quantitatively accurate estimates of component loadings and adsorption selectivities, S_{ads}, defined by

$$S_{ads} = \frac{q_1/q_2}{f_1/f_2} \tag{7}$$

As an illustration, Figure 1a presents the experimental data of Wilkins and Rajendran[2] for component loadings, q_i, of CO_2 and N_2 for adsorption of CO_2/N_2 mixtures in 13X zeolite at 296 K and total pressure p_t = 97 kPa as a function of the mole fraction of CO_2 in the bulk gas phase, y_1. The dashed lines are the IAST estimations using the experimental data on the unary isotherms. The IAST estimations of the component loadings for N_2 are not in good agreement with the experimental data. Figure 1b plots the experimental data on the CO_2/N_2 adsorption selectivity as a function of the mole fraction of CO_2 in the bulk gas phase. The IAST severely overestimates the values of S_{ads}.

Gholipour and Mofarahi[19] reported the results of a comprehensive experimental investigation of adsorption equilibrium of CO_2/CH_4 mixture adsorption in 13X zeolite; Figure 2a presents a plot of the CO_2/CH_4 adsorption selectivity as a function of the mole fraction of CO_2 in the bulk gas mixture. As compared to the experimental data, the IAST overpredicts the selectivity values to a significant extent.

For adsorption of CO_2/C_3H_8 mixtures in 13X zeolite, the experimental data of Costa et al.[20] show selectivity reversal in favor of C_3H_8 when the mole fraction of CO_2 in the bulk gas phase, y_1 > 0.8; see Figure 2b. The phenomena of selectivity reversal are not anticipated by the IAST, which expects S_{ads} > 1 over the entire composition range.

The primary objective of this article is to gain some insights into the reasons for the failure of the IAST to match the experimental data, such as that illustrated in Figures 1 and 2. Toward this end, configurational-bias Monte Carlo (CBMC) simulations for adsorption of CO_2/N_2, CO_2/CH_4, and CO_2/C_3H_8 mixtures in NaX zeolite (per unit cell: 106 Si, 86 Al, and 86 Na^+ with Si/Al = 1.23) are performed using the simulation methodology that is firmly established in the literature.[3,10,27−29] The force field information are taken from García-Sánchez et al.[30] and Dubbeldam et al.[31] The Supporting Information accompanying this publication provides (a) details of the CBMC simulation methodology, (b) unary isotherm fits for all of the guest/host combinations, (c) details of the IAST and real adsorbed solution theory (RAST) calculations for mixture adsorption equilibrium, and (d) Wilson parameter fits for thermodynamic nonidealities.

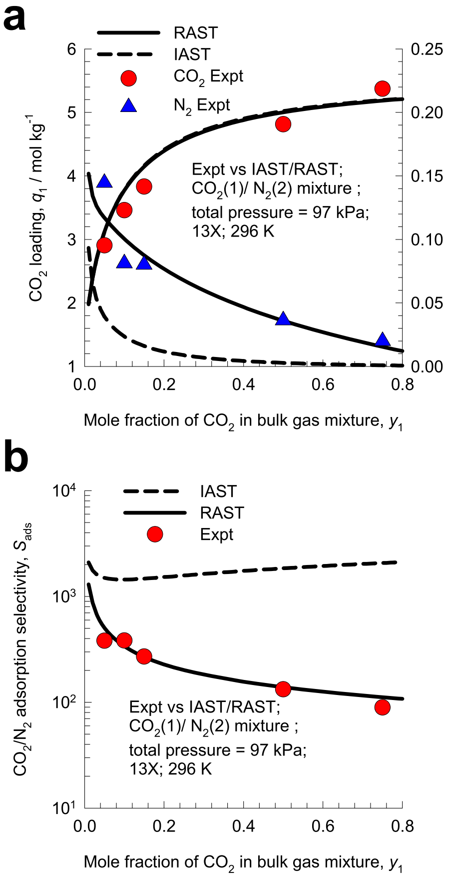

Figure 1. (a) Experimental data (indicated by symbols) of Wilkins and Rajendran[2] for component loadings, q_i, of CO_2 and N_2 for adsorption of CO_2/N_2 mixtures in 13X zeolite at 296 K and total pressure p_t = 97 kPa as a function of the mole fraction of CO_2 in the bulk gas phase. (b) CO_2/N_2 adsorption selectivity as a function of the mole fraction of CO_2 in the bulk gas phase. All calculation details and input data are provided in the Supporting Information accompanying this publication.

2. CBMC SIMULATION RESULTS AND DISCUSSION

2.1. CO_2/N_2, CO_2/CH_4, and CO_2/C_3H_8 Mixture Adsorption in NaX.

Figure 3a presents the CBMC simulation data of component loadings, q_i, of CO_2 and N_2 for adsorption of CO_2/N_2 mixtures in NaX zeolite at 300 K and total gas-phase fugacity $f_t = f_1 + f_2$ = 100 kPa, plotted as a function of the mole fraction of CO_2 in the bulk gas phase, y_1. The IAST estimations of the component loadings for N_2 are not in good agreement with the CBMC mixture simulations. Figure 3b plots the CBMC data on the CO_2/N_2 adsorption selectivity as a function of the mole fraction of CO_2 in the bulk gas phase. The

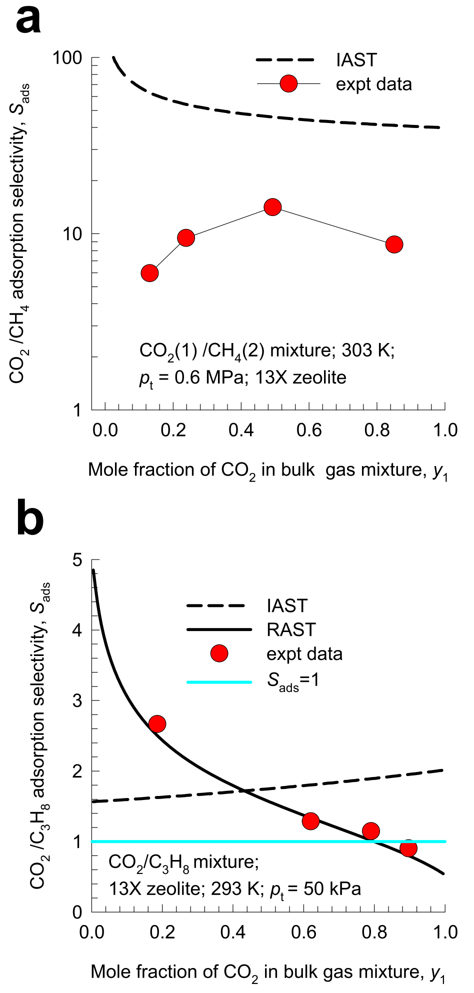

Figure 2. Comparison of experimental data on the adsorption selectivity with IAST estimates for (a) CO_2/CH_4 in 13X zeolite at T = 303 K and p_t = 0.6 MPa[19] and (b) CO_2/C_3H_8 in 13X zeolite at T = 293 K and p_t = 50 kPa.[20] The x-axis represents the mole fraction of CO_2 in the bulk gas phase, maintained at constant total pressure, p_t, and temperature, T. All calculation details and input data are provided in the Supporting Information accompanying this publication..

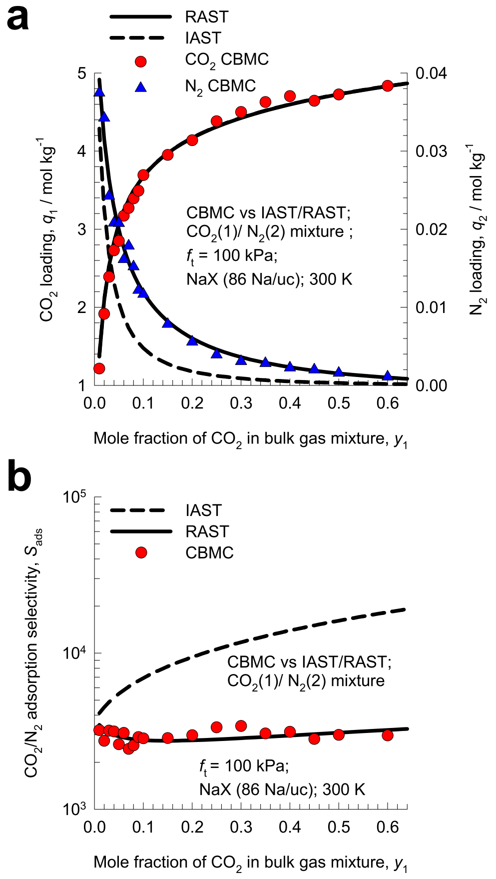

Figure 3. (a) CBMC simulation data (indicated by symbols) for component loadings, q_i, of CO_2 and N_2 for adsorption of CO_2/N_2 mixtures in NaX zeolite (106 Si, 86 Al, 86 Na^+, Si/Al = 1.23) at 300 K and total fugacity f_t = 100 kPa as a function of the mole fraction of CO_2 in the bulk gas phase, y_1. (b) CO_2/N_2 adsorption selectivity as a function of the mole fraction of CO_2 in the bulk gas phase. IAST (dashed lines) and RAST calculations (continuous solid lines) are also shown. All calculation details and input data are provided in the Supporting Information accompanying this publication.

IAST severely overestimates the adsorption selectivity, in qualitative agreement with the experimental data in Figure 1.

Figure 4a,b presents the corresponding CBMC simulation data for adsorption of CO_2/CH_4 mixtures in NaX zeolite at 300 K and total gas phase fugacity $f_t = f_1 + f_2$ = 100 kPa. The IAST overestimates the adsorption selectivity, in qualitative agreement with the experimental data in Figure 2a.

For adsorption of CO_2/C_3H_8 mixtures in NaX zeolite, CBMC simulation data for the adsorption selectivities are plotted in Figure 5 for two different total gas-phase fugacities f_t = 50 kPa and f_t = 1 MPa. The CBMC data for f_t = 50 kPa display selectivity reversals in favor of the saturated alkane for $y_1 > 0.8$, in agreement with the experimental data of Costa et al.[20] (cf. Figure 2b). The IAST calculations, shown by the dashed lines, are in poor agreement with the CBMC data and do not anticipate the selectivity reversal phenomena.

The failure of the IAST to provide a quantitative description of mixture adsorption in NaX zeolite is traceable to the use of Raoult's law analogue, eq 4, whose applicability mandates that all of the adsorption sites within the microporous material are equally accessible to each of the guest molecules, implying a homogeneous distribution of guest adsorbates within the pore landscape, with no preferential locations of any guest species. To test this requirement, CBMC simulation data on the spatial locations of the guest molecules were sampled to determine the intermolecular distances. By sampling a total of 10^5 equilibrated simulation steps, the radial distribution of the separation distances between the various molecular pairs was determined for CO_2/N_2, CO_2/CH_4, and CO_2/C_3H_8 mixtures. The data on the radial distribution functions (RDFs) are presented in Figure 6a−c. If we compare the first peaks, it is noteworthy that for all three mixtures, the CO_2-CO_2 and CO_2-Na^+ pairs are close together, indicating that the major proportion of CO_2 congregates around the cations. A further point to note is that the CO_2-N_2, CO_2-CH_4, and $CO_2-C_3H_8$ separation distances are significantly larger than the corresponding CO_2-CO_2 separation distances. This implies that the partner molecules, N_2, CH_4, and C_3H_8, endure less severe competitive adsorption with CO_2 than that anticipated by the IAST; as a consequence, the IAST overestimates the values of S_{ads}.

A visual appreciation of the congregation of CO_2 around the cations can be gained from the snapshots for CO_2/CH_4

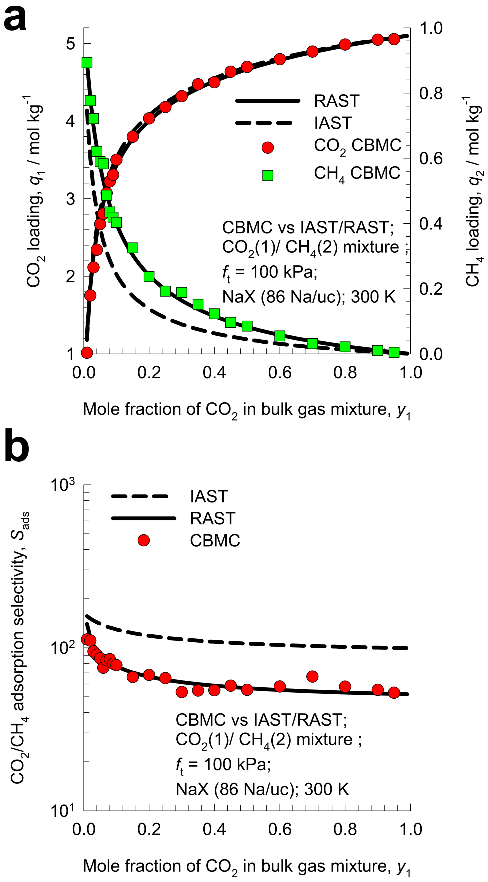

Figure 4. (a) CBMC simulation data (indicated by symbols) for component loadings, q_i, of CO$_2$ and CH$_4$ for adsorption of CO$_2$/CH$_4$ mixtures in NaX zeolite (106 Si, 86 Al, 86 Na$^+$, Si/Al = 1.23) at 300 K and total fugacity f_t = 100 kPa as a function of the mole fraction of CO$_2$ in the bulk gas phase, y_1. (b) CO$_2$/CH$_4$ adsorption selectivity as a function of the mole fraction of CO$_2$ in the bulk gas phase. IAST (dashed lines) and RAST calculations (continuous solid lines) are also shown. All calculation details and input data are provided in the Supporting Information accompanying this publication.

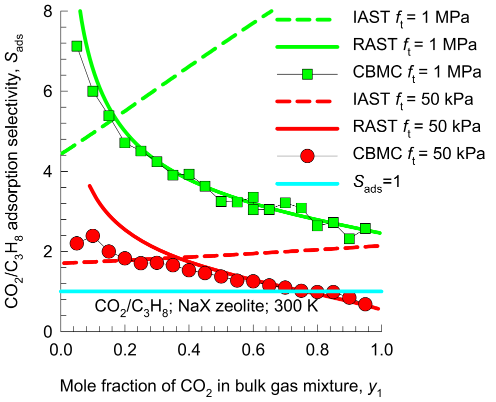

Figure 5. CBMC simulation data for adsorption of CO$_2$/C$_3$H$_8$ mixtures in NaX zeolite (106 Si, 86 Al, 86 Na$^+$, Si/Al = 1.23) at 300 K and total fugacities f_t = 50 kPa, and f_t = 1 MPa, plotted as a function of the mole fraction of CO$_2$ in the bulk gas phase, y_1. IAST (dashed lines) and RAST calculations (continuous solid lines) are also shown. All calculation details and input data are provided in the Supporting Information accompanying this publication.

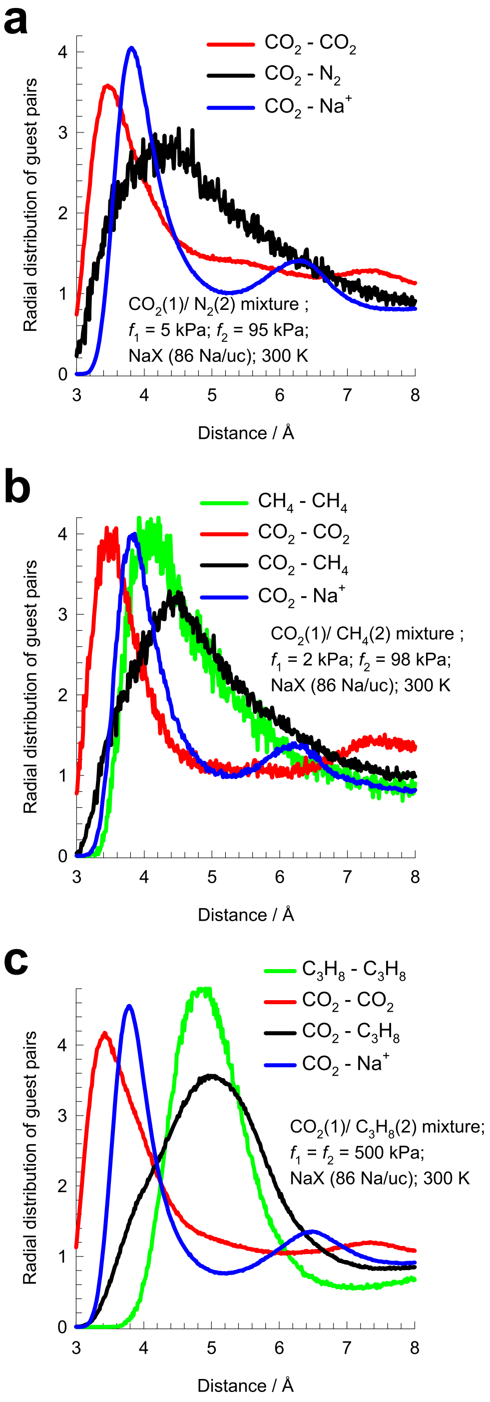

Figure 6. Radial distribution of guest pairs determined from CBMC simulations for adsorption of (a) CO$_2$/N$_2$, (b) CO$_2$/CH$_4$, and (c) CO$_2$/C$_3$H$_8$ mixtures in NaX zeolite (106 Si, 86 Al, 86 Na$^+$, and Si/Al = 1.23) at 300 K. The samples are taken up to a radial distance of 12 Å, but the x-axis has been truncated at 8 Å because only the first peaks are of interest in the discussions. All simulation details are provided in the Supporting Information accompanying this publication.

mixtures presented in Figure 7. It is also noteworthy that the CH$_4$ are further removed from the CO$_2$ guests.

Since the primary reason for the congregation of CO$_2$ molecules is the presence of cations, we should expect that for mixture adsorption in all-silica zeolites without extra-framework cations (i.e., with Si/Al → ∞), there would be no congregation or segregation effects. To confirm this expect-

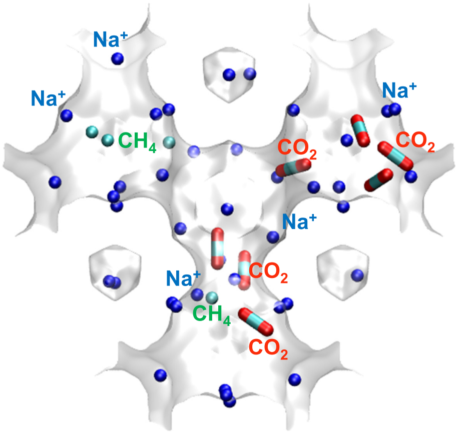

Figure 7. Snapshot showing the location of CO_2, CH_4, and Na+ cations within the pore landscape of NaX (106 Si, 86 Al, 86 Na^+, Si/Al = 1.23) zeolite at 300 K, total fugacity f_t = 100 kPa, and y_1 = 0.02.

ation, we also examined the radial distribution of adsorbates for CO_2/N_2 and CO_2/CH_4 mixtures in all-silica FAU zeolites; see Figure 8a,b. For both mixtures, the first peaks of the CO_2−CO_2, CO_2−partner, and partner−partner pairs occur at nearly the same separation distances. This indicates that there are no congregation/segregation effects and that the guest molecules are homogeneously distributed within the pore landscape. Such a homogeneous distribution of guest molecules fulfills the requirement of the IAST. Consequently, we should expect the IAST to provide a good quantitative description of CO_2/N_2 and CO_2/CH_4 mixture adsorption in all-silica zeolites. To confirm this expectation, we performed CBMC simulations for adsorption of 15/85 CO_2/N_2 and 50/50 CO_2/CH_4 mixtures in all-silica FAU, in which the total fugacity of the bulk gas phase mixture $f_t = f_1 + f_2$ is varied from 10^2 Pa to 10^7 Pa. Figure 9a,b compares the CBMC simulated values of the adsorption selectivities with the corresponding IAST calculations; there is excellent agreement between the two data sets. In sharp contrast, the IAST calculations severely overpredict the adsorption selectivities for both mixtures in NaX zeolite. Evidence of inhomogeneous distribution of adsorbates in other zeolites such as LTA-4A and DDR is provided in Figures S29−S33 of the Supporting Information.

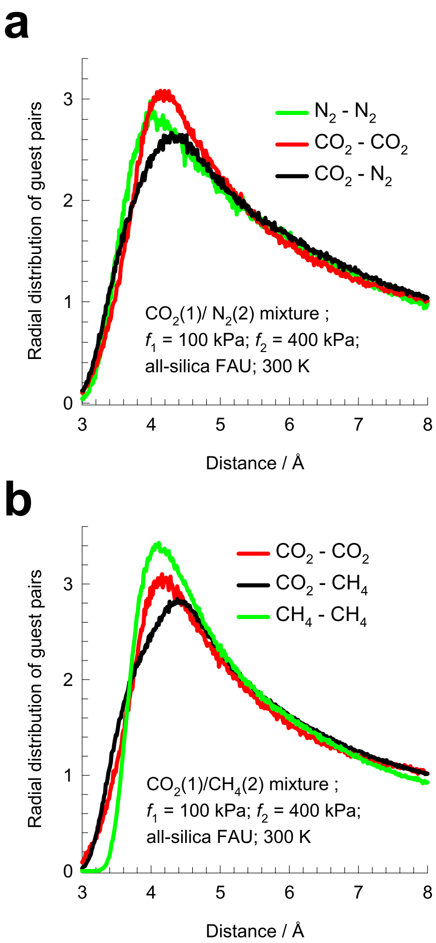

Figure 8. Radial distribution of guest pairs determined from CBMC simulations for adsorption of (a) CO_2/N_2 and (b) CO_2/CH_4 mixtures in all-silica FAU zeolite (192 Si, 0 Al, 0 Na^+, Si/Al = ∞) at 300 K.

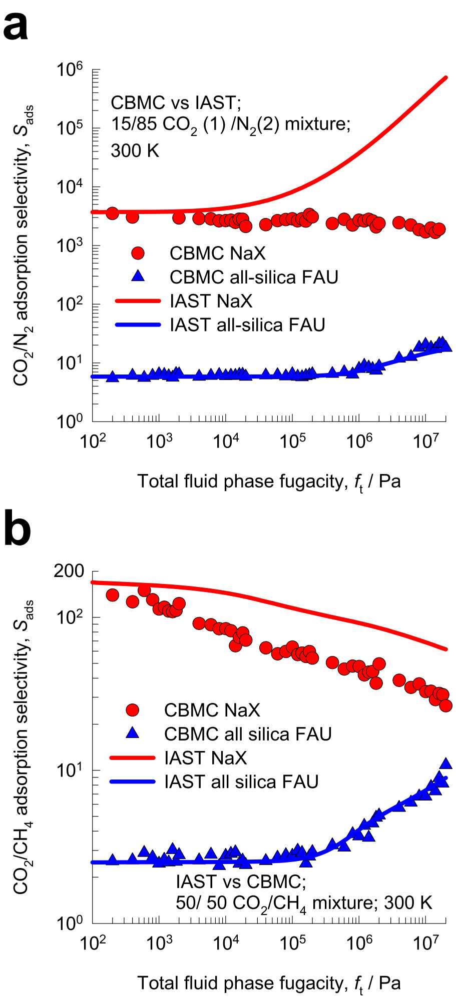

Figure 9. Comparisons of CBMC simulated values of adsorption selectivities for (a) 15/85 CO_2/N_2 and (b) 50/50 CO_2/CH_4 mixtures determined from CBMC simulations for all-silica FAU (192 Si, 0 Al, 0 Na^+, Si/Al = ∞) and NaX (106 Si, 86 Al, 86 Na^+, Si/Al = 1.23) at 300 K with IAST estimations. The *x*-axis is the total fugacity of the bulk gas phase mixture, $f_t = f_1 + f_2$.

2.2. Modeling Nonidealities for Mixture Adsorption.

For quantitative modeling of nonideality effects in mixture adsorption arising out of congregation/segregation effects, we need to introduce activity coefficients γ_i in eq (4)

$$f_i = \gamma_i x_i P_i^0 \tag{8}$$

The implementation of the activity coefficients is termed as the real adsorbed solution theory (RAST). For parametrization of the activity coefficients, the well-known Wilson model for vapor−liquid equilibria can be adapted for binary mixture adsorption as follows

$$\begin{aligned}\ln(\gamma_1) &= \left(1 - \ln(x_1 + x_2\Lambda_{12}) - \frac{x_1}{x_1 + x_2\Lambda_{12}} - \frac{x_2\Lambda_{21}}{x_2 + x_1\Lambda_{21}}\right)\left(1 - \exp\left(-C\frac{\pi A}{RT}\right)\right)\\ \ln(\gamma_2) &= \left(1 - \ln(x_1\Lambda_{21} + x_2) - \frac{x_1\Lambda_{12}}{x_1 + x_2\Lambda_{12}} - \frac{x_2}{x_1\Lambda_{21} + x_2}\right)\left(1 - \exp\left(-C\frac{\pi A}{RT}\right)\right)\end{aligned} \tag{9}$$

The introduction of $\left(1 - \exp\left(-C\frac{\pi A}{RT}\right)\right)$, where C is a constant with the unit kg mol^{-1}, imparts the correct limiting behaviors $\gamma_i \to 1$; $\frac{\pi A}{RT} \to 0$ for the activity coefficients in the Henry regime, $f_t \to 0$; $\frac{\pi A}{RT} \to 0$. The three parameters Λ_{12},Λ_{21}, and C can be determined by fitting experimental or CBMC simulated data sets. For the CBMC simulated data for $CO_2(1)/N_2(2)$ mixture adsorption in NaX (cf. Figure 3a), the fitted Wilson parameters are $\Lambda_{12} = 8.6$, $\Lambda_{21} = 0.12$, and $C = 0.025$ mol kg^{-1}, and Figure 10a presents the RAST calculations of the activity coefficients. It is noteworthy that γ_1 is practially unity over the entire composition range, implying that congregation effects have practically no influence on CO_2 adsorption. On the other hand, γ_2 shows increasing departure from unity as the mole fraction of CO_2 in the bulk gas phase, y_1, increases. The inhomogeneous distribution of adsorbates influences the adsorption of N_2 to a significant extent. Analogous results are obtained for $CO_2(1)/CH_4(2)$ mixture adsorption; see Figure 10b. For CO_2/C_3H_8 mixtures, thermodynamic nonidealities influence the adsorption of both guests, and both γ_1 and γ_2 have values lower than unity; see Figure 10c.

The RAST calculations of mixture adsorption are shown by the continuous solid lines in Figures 1−4. For CO_2/C_3H_8 mixtures, the RAST calculations in Figure 5 for both $f_t = 50$ kPa and $f_t = 1$ MPa are obtained with the same set of fitted Wilson parameters $\Lambda_{12} = 1.5$, $\Lambda_{21} = 2.4$, and $C = 1$ mol kg^{-1}; the selectivity reversal phenomena at $f_t = 50$ kPa arise "naturally" out of thermodynamic nonidealities.

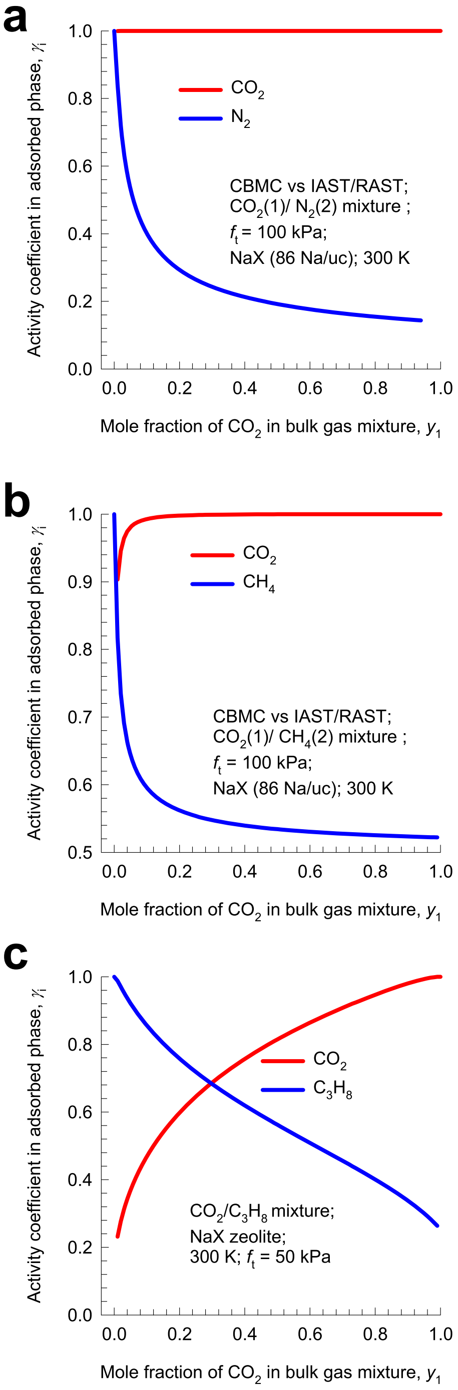

Figure 10. RAST calculations of the activity coefficients for adsorption of (a) CO_2/N_2, (b) CO_2/CH_4, and (c) CO_2/C_3H_8 mixtures in NaX zeolite at 300 K. All calculation details and input data on the Wilson parameters are provided in the Supporting Information accompanying this publication.

3. CONCLUSIONS

The failure of the IAST to provide quantitative estimates of component loadings and selectivities for CO_2/CH_4, CO_2/N_2, and CO_2/C_3H_8 mixture adsorption in NaX zeolite has been investigated and elucidated with the aid of CBMC simulations. CBMC simulations have been used to determine the intermolecular distances for each pair of guest species. The obtained radial distributions reveal that there is congregation of CO_2 around the extra-framework cations, causing an inhomogeneous distribution of adsorbates in the pore space. Partner molecules such as N_2, CH_4, and C_3H_8 are further removed from the CO_2 molecules and thereby face less severe competition during mixture adsorption. As a consequence, the IAST generally overestimates the selectivity for adsorption of CO_2. For CO_2/C_3H_8 mixture adsorption, the inhomogeneous distribution of adsorbates leads to selectivity reversals, which have been established in both experiments (Figure 2b) and simulations (Figure 5).

The important message that emerges from this investigation is the need to incorporate the RAST for quantitative modeling of fixed-bed adsorbers in CO_2 capture applications.

■ ASSOCIATED CONTENT

Supporting Information

The Supporting Information is available free of charge at https://pubs.acs.org/doi/10.1021/acsomega.0c02730.

> Provides (a) structural details of zeolites, (b) details of the CBMC simulation methodology, (c) unary isotherm fits for all of the guest/host combinations, (d) details of the IAST and real adsorbed solution theory (RAST) calculations for mixture adsorption equilibrium, and (d) Wilson parameter fits for thermodynamic nonidealities (PDF)

■ AUTHOR INFORMATION

Corresponding Author

Rajamani Krishna − *Van't Hoff Institute for Molecular Sciences, University of Amsterdam, 1098 XH Amsterdam, The Netherlands;* orcid.org/0000-0002-4784-8530; Email: r.krishna@contact.uva.nl

Author

Jasper M. van Baten − *Van't Hoff Institute for Molecular Sciences, University of Amsterdam, 1098 XH Amsterdam, The Netherlands*

Complete contact information is available at: https://pubs.acs.org/10.1021/acsomega.0c02730

Notes

The authors declare no competing financial interest.

■ ACKNOWLEDGMENTS

The authors acknowledge Dr. Richard Baur for helpful discussions.

■ NOMENCLATURE

Latin Alphabet

A	surface area per kg of framework, m^2 kg^{-1}
C	constant used in eq 9, kg mol^{-1}
f_i	partial fugacity of species i, Pa
f_t	total fugacity of bulk fluid mixture, Pa
n	number of species in the mixture, dimensionless
p_i	partial pressure of species i, Pa
p_t	total system pressure, Pa
P_i^0	sorption pressure, Pa
q_i	molar loading of species i, mol kg^{-1}
q_t	total molar loading of mixture, mol kg^{-1}
R	gas constant, 8.314 J mol^{-1} K^{-1}
S_{ads}	adsorption selectivity, dimensionless
T	absolute temperature, K
x_i	mole fraction of species i in the adsorbed phase, dimensionless
y_i	mole fraction of species i in the bulk fluid mixture, dimensionless

■ GREEK ALPHABET

γ_i	activity coefficient of component i in the adsorbed phase, dimensionless
Λ_{ij}	Wilson parameters, dimensionless
μ_i	molar chemical potential, J mol^{-1}
π	spreading pressure, N m^{-1}

■ REFERENCES

(1) Pirngruber, G. D.; Carlier, V.; Leinekugel-le-Cocq, D. Post-Combustion CO_2 Capture by Vacuum Swing Adsorption Using Zeolites – a Feasibility Study. *Oil Gas Sci. Technol.* **2014**, *69*, 989−1003.

(2) Wilkins, N. S.; Rajendran, A. Measurement of competitive CO_2 and N_2 adsorption on Zeolite 13X for post-combustion CO_2 capture. *Adsorption* **2019**, *25*, 115−133.

(3) Krishna, R.; van Baten, J. M. A comparison of the CO_2 capture characteristics of zeolites and metal-organic frameworks. *Sep. Purif. Technol.* **2012**, *87*, 120−126.

(4) Krishna, R. Metrics for Evaluation and Screening of Metal-Organic Frameworks for Applications in Mixture Separations. *ACS Omega* **2020**, *5*, 16987−17004.

(5) Ruthven, D. M.; Farooq, S.; Knaebel, K. S. *Pressure Swing Adsorption*; VCH Publishers: New York, 1994.

(6) Krishna, R. Screening Metal-Organic Frameworks for Mixture Separations in Fixed-Bed Adsorbers using a Combined Selectivity/Capacity Metric. *RSC Adv.* **2017**, *7*, 35724−35737.

(7) Yang, R. T. *Gas Separation by Adsorption Processes*; Butterworth: Boston, 1987.

(8) Mason, J. A.; Sumida, K.; Herm, Z. R.; Krishna, R.; Long, J. R. Evaluating Metal-Organic Frameworks for Post-Combustion Carbon Dioxide Capture via Temperature Swing Adsorption. *Energy Environ. Sci.* **2011**, *4*, 3030−3040.

(9) Xiang, S. C.; He, Y.; Zhang, Z.; Wu, H.; Zhou, W.; Krishna, R.; Chen, B. Microporous Metal-Organic Framework with Potential for Carbon Dioxide Capture at Ambient Conditions. *Nat. Commun.* **2012**, *3*, No. 954.

(10) Krishna, R.; van Baten, J. M. In silico screening of metal-organic frameworks in separation applications. *Phys. Chem. Chem. Phys.* **2011**, *13*, 10593−10616.

(11) Wu, H.; Yao, K.; Zhu, Y.; Li, B.; Shi, Z.; Krishna, R.; Li, J. Cu-TDPAT, an *rht*-type Dual-Functional Metal−Organic Framework Offering Significant Potential for Use in H_2 and Natural Gas Purification Processes Operating at High Pressures. *J. Phys. Chem. C* **2012**, *116*, 16609−16618.

(12) Belmabkhout, Y.; Pirngruber, G.; Jolimaitre, E.; Methivier, A. A complete experimental approach for synthesis gas separation studies using static gravimetric and column breakthrough experiments. *Adsorption* **2007**, *13*, 341−349.

(13) He, Y.; Krishna, R.; Chen, B. Metal-Organic Frameworks with Potential for Energy-Efficient Adsorptive Separation of Light Hydrocarbons. *Energy Environ. Sci.* **2012**, *5*, 9107−9120.

(14) Myers, A. L.; Prausnitz, J. M. Thermodynamics of Mixed Gas Adsorption. *AIChE J.* **1965**, *11*, 121−130.

(15) Ruthven, D. M. *Principles of Adsorption and Adsorption Processes*; John Wiley: New York, 1984.

(16) Krishna, R.; van Baten, J. M.; Baur, R. Highlighting the Origins and Consequences of Thermodynamic Nonidealities in Mixture Separations using Zeolites and Metal-Organic Frameworks. *Microporous Mesoporous Mater.* **2018**, *267*, 274−292.

(17) Krishna, R.; Van Baten, J. M. Investigating the Non-idealities in Adsorption of CO_2-bearing Mixtures in Cation-exchanged Zeolites. *Sep. Purif. Technol.* **2018**, *206*, 208−217.

(18) Mofarahi, M.; Gholipour, F. Gas Adsorption Separation of CO_2/CH_4 System using Zeolite 5A. *Microporous Mesoporous Mater.* **2014**, *200*, 47−54.

(19) Gholipour, F.; Mofarahi, M. Adsorption Equilibrium of Methane and Carbon Dioxide on Zeolite13X: Experimental and Thermodynamic Modeling. *J. Supercrit. Fluids* **2016**, *111*, 47−54.

(20) Costa, E.; Calleja, G.; Jimenez, A.; Pau, J. Adsorption Equilibrium of Ethylene, Propane, Propylene, Carbon Dioxide, and Their Mixtures in 13X Zeolite. *J. Chem. Eng. Data* **1991**, *36*, 218−224.

(21) Siperstein, F. R.; Myers, A. L. Mixed-Gas Adsorption. *AIChE J.* **2001**, *47*, 1141−1159.

(22) Talu, O.; Zwiebel, I. Multicomponent Adsorption Equilibria of Nonideal Mixtures. *AIChE J.* **1986**, *32*, 1263−1276.

(23) Hefti, M.; Marx, D.; Joss, L.; Mazzotti, M. Adsorption Equilibrium of Binary Mixtures of Carbon Dioxide and Nitrogen on Zeolites ZSM-5 and 13X. *Microporous Mesoporous Mater.* **2015**, *215*, 215−228.

(24) Krishna, R.; Van Baten, J. M. Elucidation of Selectivity Reversals for Binary Mixture Adsorption in Microporous Adsorbents. *ACS Omega* **2020**, *5*, 9031−9040.

(25) van Zandvoort, I.; Ras, E.-J.; de Graaf, R.; Krishna, R. Using Transient Breakthrough Experiments for Screening of Adsorbents for Separation of C_2H_4/CO_2 Mixtures. *Sep. Purif. Technol.* **2020**, *241*, No. 116706.

(26) van Zandvoort, I.; van der Waal, J. K.; Ras, E.-J.; de Graaf, R.; Krishna, R. Highlighting non-idealities in C_2H_4/CO_2 mixture adsorption in 5A zeolite. *Sep. Purif. Technol.* **2019**, *227*, No. 115730.

(27) Frenkel, D.; Smit, B. *Understanding Molecular Simulations: From Algorithms to Applications*, 2nd ed.; Academic Press: San Diego, 2002.

(28) Smit, B.; Krishna, R. Molecular simulations in zeolitic process design. *Chem. Eng. Sci.* **2003**, *58*, 557−568.

(29) Vlugt, T. J. H.; Krishna, R.; Smit, B. Molecular Simulations of Adsorption Isotherms for Linear and Branched Alkanes and Their Mixtures in Silicalite. *J. Phys. Chem. B* **1999**, *103*, 1102−1118.

(30) García-Sánchez, A.; Ania, C. O.; Parra, J. B.; Dubbeldam, D.; Vlugt, T. J. H.; Krishna, R.; Calero, S. Development of a Transferable Force Field for Carbon Dioxide Adsorption in Zeolites. *J. Phys. Chem. C* **2009**, *113*, 8814−8820.

(31) Dubbeldam, D.; Calero, S.; Vlugt, T. J. H.; Krishna, R.; Maesen, T. L. M.; Smit, B. United Atom Forcefield for Alkanes in Nanoporous Materials. *J. Phys. Chem. B* **2004**, *108*, 12301−12313.

Supporting Information

Using Molecular Simulations for Elucidation of Thermodynamic Non-Idealities in Adsorption of CO_2-containing Mixtures in NaX Zeolite

Rajamani Krishna* and Jasper M. van Baten

Van 't Hoff Institute for Molecular Sciences
University of Amsterdam
Science Park 904
1098 XH Amsterdam, The Netherlands
email: r.krishna@contact.uva.nl

Table of Contents

1 Preamble

This Supplementary material accompanying our manuscript *Using Molecular Simulations for Elucidation of Thermodynamic Non-Idealities in Adsorption of* CO_2*-containing Mixtures in NaX Zeolite* provides (a) details of the CBMC simulation methodology, (b) unary isotherm fits for all the guest/host combinations, (c) details of the IAST, and Real Adsorbed Solution Theory (RAST) calculations for mixture adsorption equilibrium, and (d) Wilson parameter fits for thermodynamic non-idealities.

2 Configurational-Bias Monte Carlo Simulation Methodology

The simulation methodologies and the force field information used are the same as detailed in the Supplementary Materials accompanying our earlier publications.[1-7] A short summary is provided hereunder.

2.1 Zeolites (all silica)

CH_4 molecules are described with a united atom model, in which each molecule is treated as a single interaction center.[8] The interaction between adsorbed molecules is described with Lennard-Jones terms. The Lennard-Jones parameters for CH_4-zeolite interactions are taken from Dubbeldam et al.[9]. The Lennard-Jones parameters for CO_2-zeolite and N_2-zeolite are those reported by García-Pérez et al.[10] For simulations with linear alkanes with two or more C atoms, the beads in the chain are connected by harmonic bonding potentials; see Figure S1. A harmonic cosine bending potential models the bond bending between three neighboring beads, a Ryckaert-Bellemans potential controls the torsion angle. The beads in a chain separated by more than three bonds interact with each other through a Lennard-Jones potential; see schematic in Figure S1. The force fields of Dubbeldam et al.[9] was used for the variety of potentials. The Lennard-Jones potentials are shifted and cut at 12 Å.

The zeolite frameworks were considered to be rigid in all the simulation results reported in the article.

All-silica FAU (= faujasite) has cages of 786 $Å^3$ volume, separated by 7.3 Å 12-ring windows; see structural information in Figure S2, and Figure S3.

Figure S4 shows the structural details of NaX (= 86 Na^+/uc = 13X) zeolite. Per unit cell of NaX zeolite we have 106 Si, 86 Al, 86 Na^+ with Si/Al=1.23. This material is also commonly referred to by its trade name: 13X zeolite.

DDR consists of cages of 277.8 Å^3 volume, separated by 3.65 Å × 4.37 Å 8-ring windows; the pore landscapes and structural details are provided in Figure S5, and Figure S6.

LTA, LTA-5A, and LTA-4A consist of cages of 743 Å^3 volume, separated by 4.11 Å × 4.47 Å 8-ring windows; the pore landscapes and structural details are provided in Figure S7, Figure S8. Figure S9, and Figure S10.

Per unit cell, LTA-5 has 96 Si, 96 Al, 32 Na$^+$, 32 Ca^{++} with Si/Al=1.

Per unit cell LTA-4A has 96 Si, 96 Al, 96 Na$^+$, Si/Al=1.

The force field information for the simulations with cations are taken from García-Sanchez et al.[11] In the MC simulations, the cations were allowed to move within the framework and both Lennard-Jones and Coulombic interactions are taken into consideration.

In the CBMC simulations both Lennard-Jones and Coulombic interactions are taken into consideration; see schematic sketch in Figure S11.

.

2.2 List of Figures for Configurational-Bias Monte Carlo Simulation Methodology

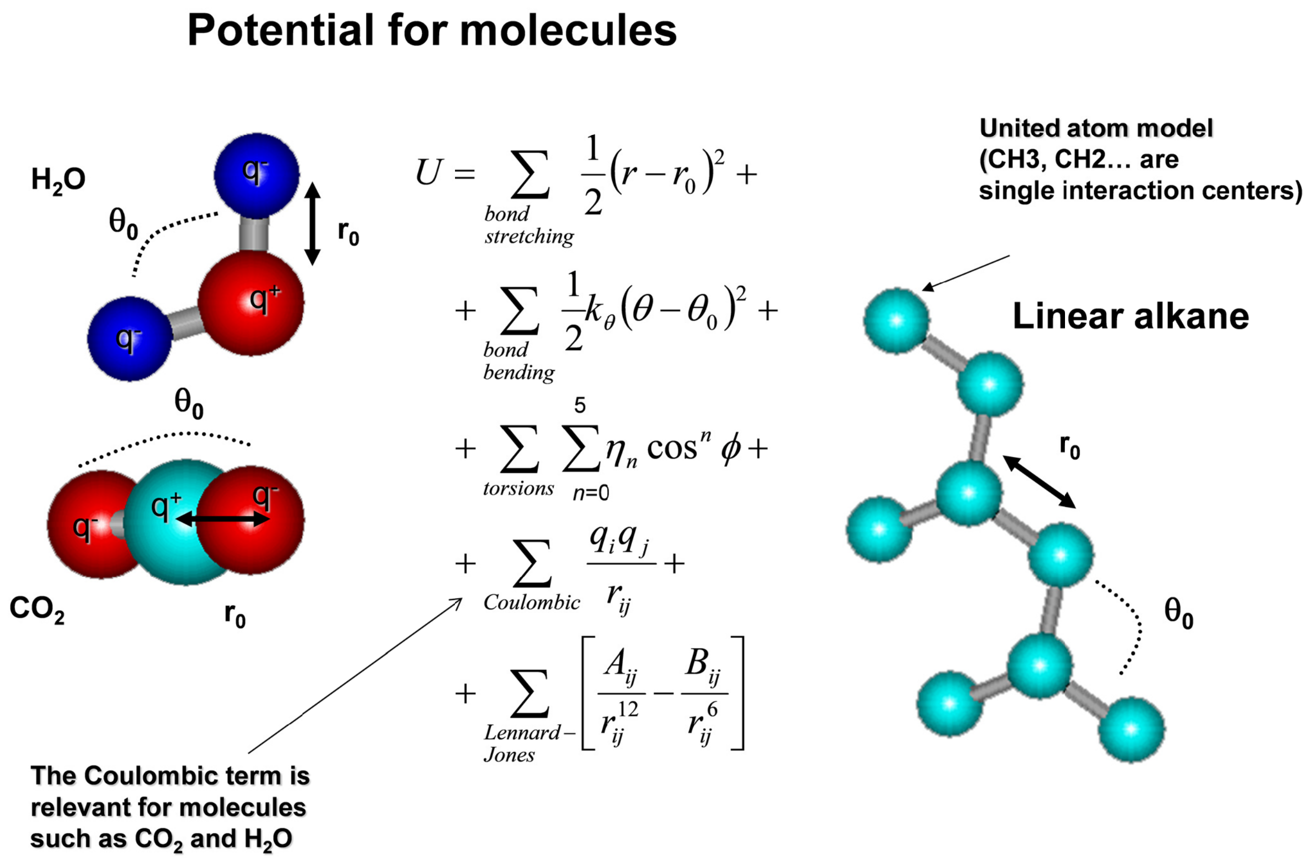

Potential for molecules

$$U = \sum_{\substack{bond\\stretching}} \frac{1}{2}(r-r_0)^2 + \sum_{\substack{bond\\bending}} \frac{1}{2}k_\theta(\theta-\theta_0)^2 + \sum_{torsions} \sum_{n=0}^{5} \eta_n \cos^n \phi + \sum_{Coulombic} \frac{q_i q_j}{r_{ij}} + \sum_{Lennard-Jones} \left[\frac{A_{ij}}{r_{ij}^{12}} - \frac{B_{ij}}{r_{ij}^{6}} \right]$$

United atom model (CH3, CH2… are single interaction centers)

The Coulombic term is relevant for molecules such as CO_2 and H_2O

Figure S1. Potential for molecules.

FAU-Si pore landscape

The sodalite cages are blocked in simulations and are not accessible to guest molecules; these are excluded for pore volume determination.

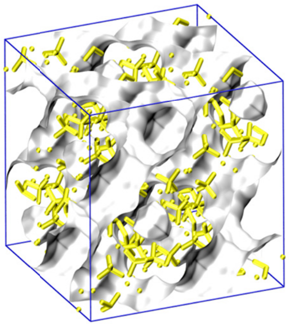

12-ring window of FAU

There are 8 cages per unit cell. The volume of one FAU cage is 786 Å^3, larger in size than that of LTA (743 Å^3) and DDR (278 Å^3).

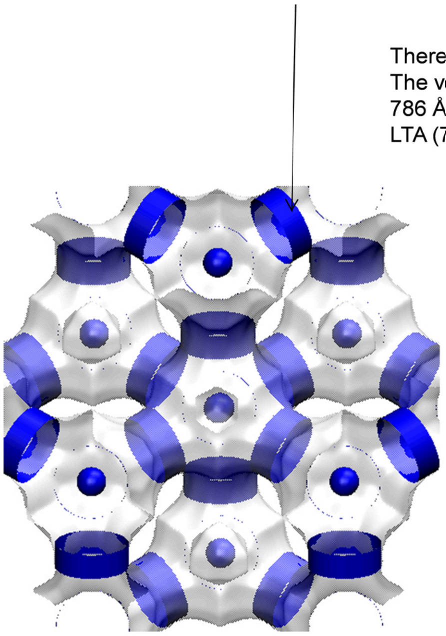

Structural information from: C. Baerlocher, L.B. McCusker, Database of Zeolite Structures, International Zeolite Association, http://www.iza-structure.org/databases/

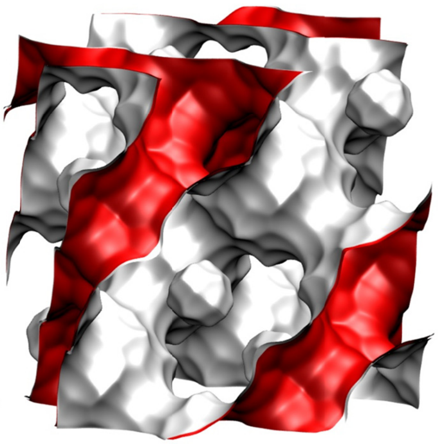

Figure S2. Pore landscape of all-silica FAU zeolite.

FAU-Si window and pore dimensions

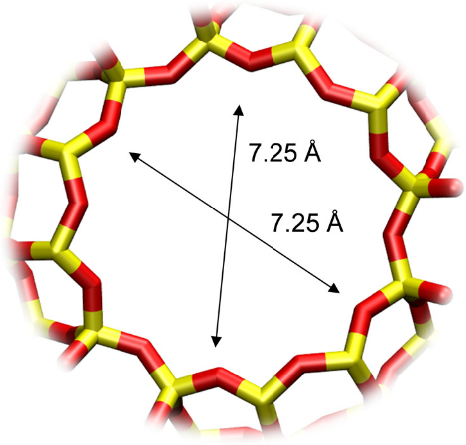

	FAU-Si
a /Å	24.28
b /Å	24.28
c /Å	24.28
Cell volume / Å^3	14313.51
conversion factor for [molec/uc] to [mol per kg Framework]	0.0867
conversion factor for [molec/uc] to [kmol/m^3]	0.2642
ρ [kg/m3]	1338.369
MW unit cell [g/mol (framework)]	11536.28
ϕ, fractional pore volume	0.439
open space / Å^3/uc	6285.6
Pore volume / cm^3/g	0.328
Surface area /m^2/g	1086.0
DeLaunay diameter /Å	7.37

Figure S3. Structural details for FAU zeolite.

NaX (106 Si, 86 Al, 86 Na+, Si/Al=1.23)

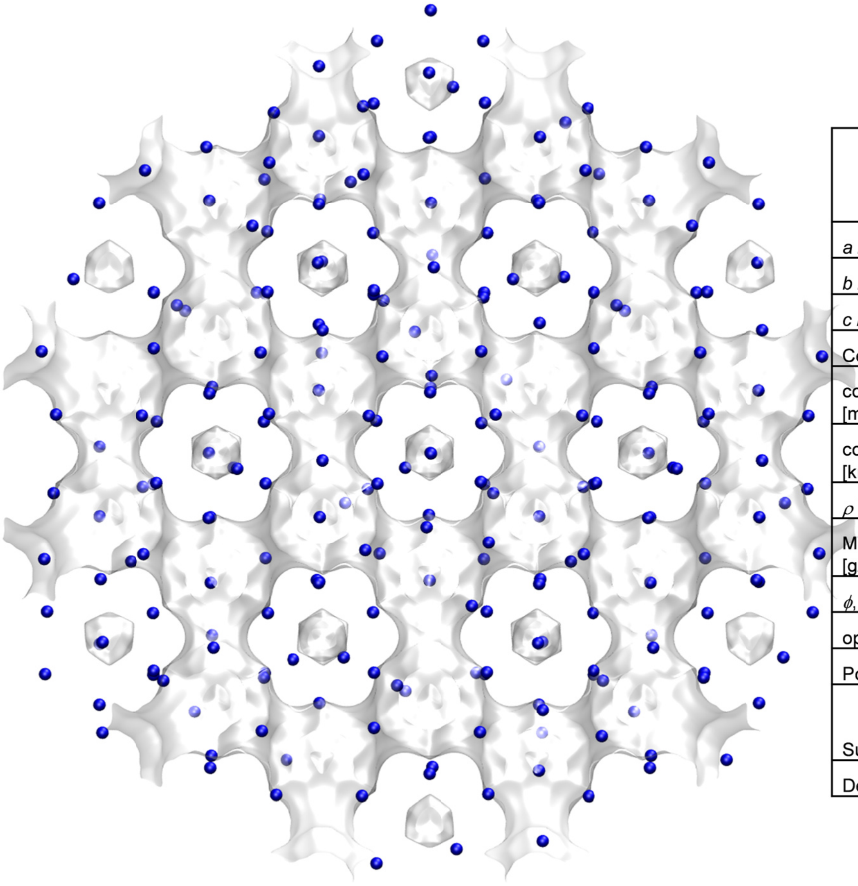

	FAU 86 Na/uc
a /Å	25.028
b /Å	25.028
c /Å	25.028
Cell volume / Å^3	15677.56
conversion factor for [molec/uc] to [mol per kg Framework]	0.0745
conversion factor for [molec/uc] to [kmol/m^3]	0.2658
ρ [kg/m3] (with cations)	1421.277
MW unit cell [g/mol(framework+cations)]	13418.42
ϕ, fractional pore volume	0.399
open space / Å^3/uc	6248.0
Pore volume / cm^3/g	0.280
Surface area /m^2/g	
DeLaunay diameter /Å	7.37

Figure S4. Location of cations for NaX zeolite (106 Si, 86 Al, 86 Na$^+$, Si/Al=1.23)

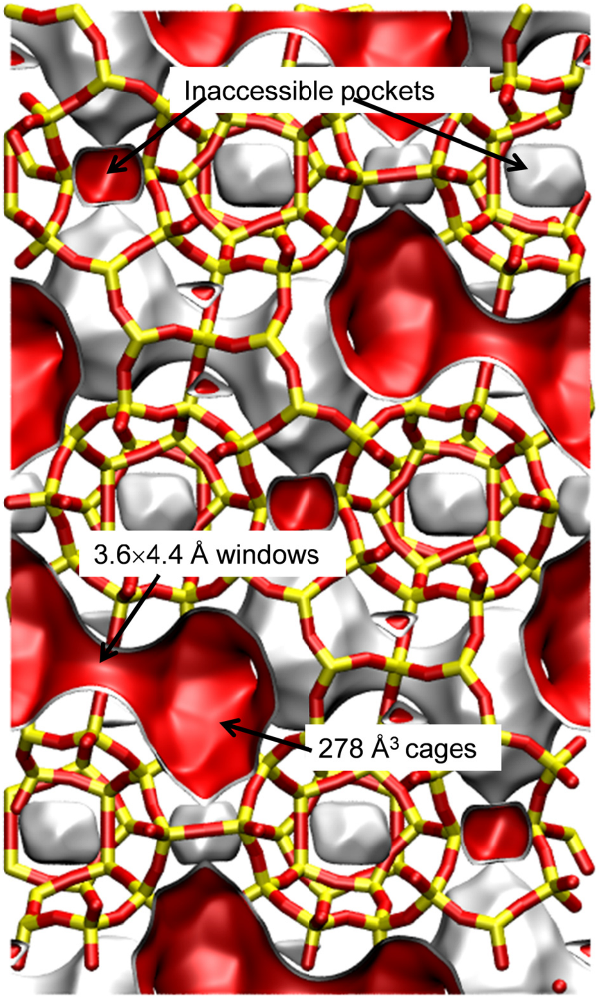

DDR landscape

To convert from molecules per unit cell to mol kg^{-1}, multiply by 0.06936.
The pore volume is 0.182 cm^3/g.

There are 12 cages per unit cell. The volume of one DDR cage is 278 Å^3, significantly smaller than that of a single cage of FAU (786 Å^3), or ZIF-8 (1168 Å^3).

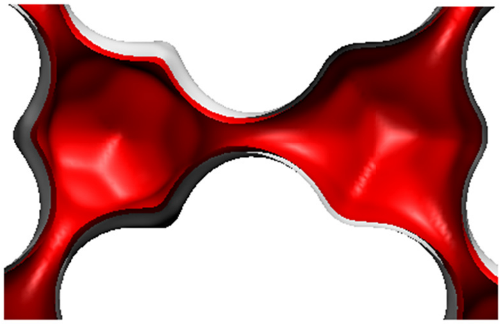

Structural information from: C. Baerlocher, L.B. McCusker, Database of Zeolite Structures, International Zeolite Association, http://www.iza-structure.org/databases/

Figure S5. Pore landscape of all-silica DDR zeolite.

DDR window and pore dimensions

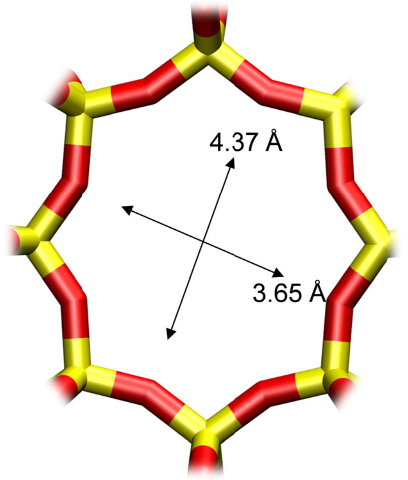

DDR

The window dimensions calculated using the van der Waals diameter of framework atoms = 2.7 Å are indicated above by the arrows.

	DDR
a /Å	24.006
b /Å	13.86
c /Å	40.892
Cell volume / Å^3	13605.72
conversion factor for [molec/uc] to [mol per kg Framework]	0.0693
conversion factor for [molec/uc] to [kmol/m^3]	0.4981
ρ [kg/m3]	1759.991
MW unit cell [g/mol(framework)]	14420.35
ϕ, fractional pore volume	0.245
open space / Å^3/uc	3333.5
Pore volume / cm^3/g	0.139
Surface area /m^2/g	350.0
DeLaunay diameter /Å	3.65

Figure S6. Structural details for DDR zeolite.

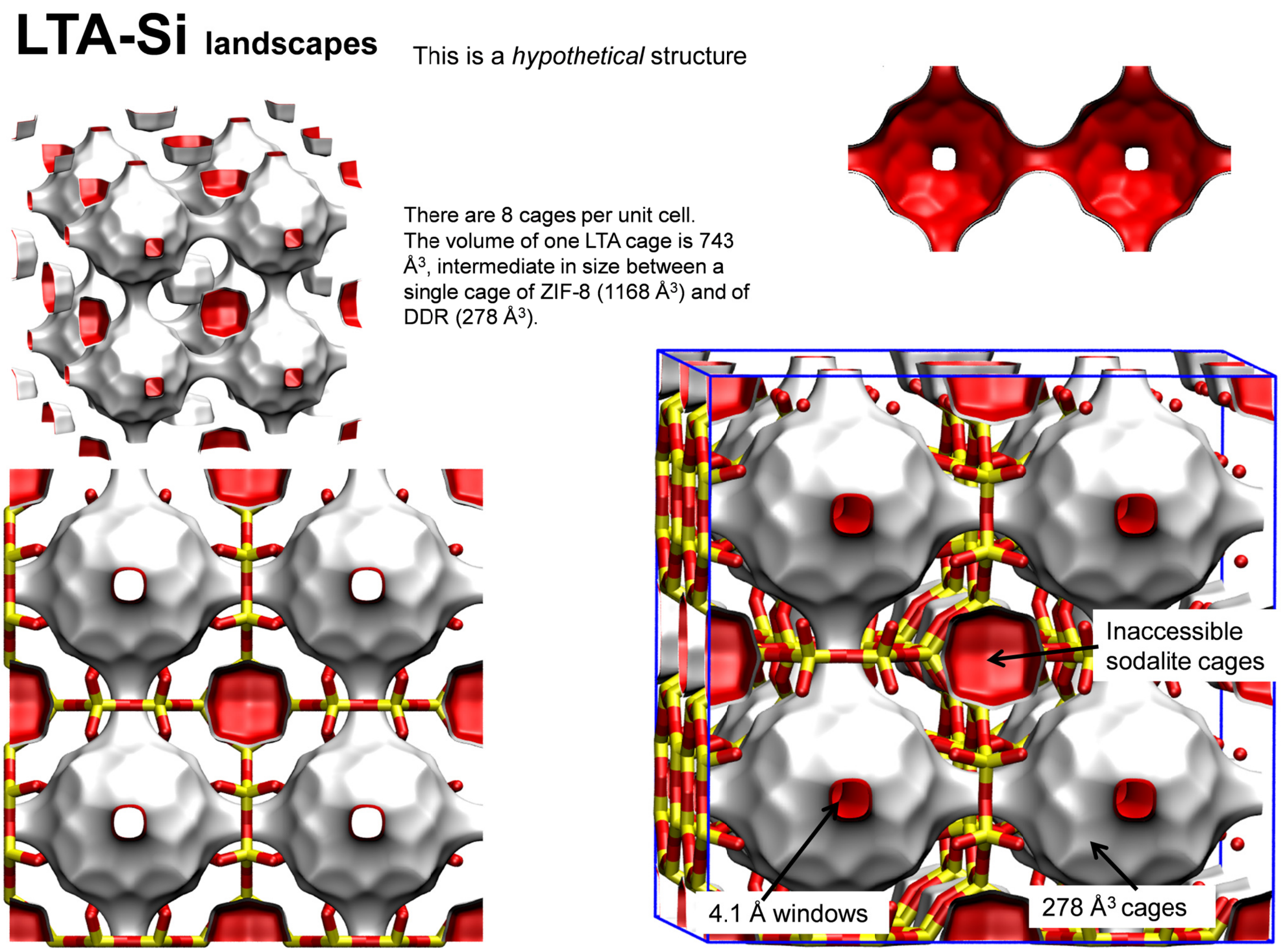

This is a *hypothetical* structure

There are 8 cages per unit cell. The volume of one LTA cage is 743 Å^3, intermediate in size between a single cage of ZIF-8 (1168 Å^3) and of DDR (278 Å^3).

Figure S7. Pore landscape of all-silica LTA zeolite.

LTA-Si window and pore dimensions

8-ring window of LTA

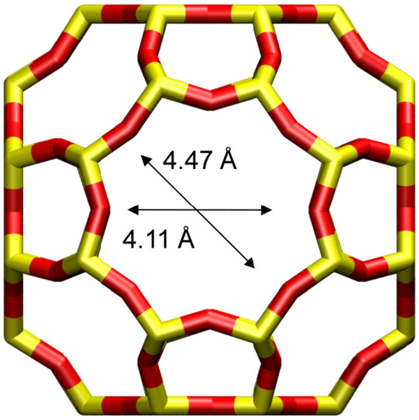

The window dimension calculated using the van der Waals diameter of framework atoms = 2.7 Å is indicated above by the arrows.

	LTA-Si
a /Å	24.61
b /Å	24.61
c /Å	24.61
Cell volume / Å^3	14905.1
conversion factor for [molec/uc] to [mol per kg Framework]	0.0867
conversion factor for [molec/uc] to [kmol/m^3]	0.2794
ρ [kg/m3]	1285.248
MW unit cell [g/mol(framework)]	11536.28
ϕ, fractional pore volume	0.399
open space / Å^3/uc	5944.4
Pore volume / cm^3/g	0.310
Surface area /m^2/g	896.0
DeLaunay diameter /Å	4.10

Figure S8. Structural details for all-silica LTA zeolite.

LTA-5A

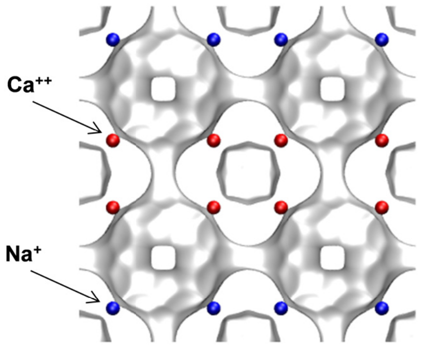

LTA-5A (32 Na+, 32 Ca++)

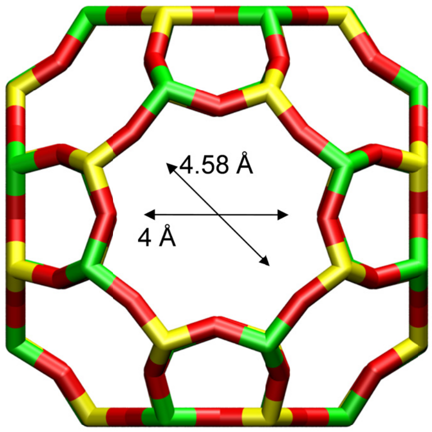

LTA-5A

The window dimension calculated using the van der Waals diameter of framework atoms = 2.7 Å is indicated above by the arrow.

	LTA-5A
a /Å	24.555
b /Å	24.555
c /Å	24.555
Cell volume / Å^3	14805.39
conversion factor for [molec/uc] to [mol per kg Framework]	0.0744
conversion factor for [molec/uc] to [kmol/m^3]	0.2955
ρ [kg/m3] (with cations)	1508.376
MW unit cell [g/mol(framework+cations)]	13448.48
ϕ, fractional pore volume	0.380
open space / Å^3/uc	5620.4
Pore volume / cm^3/g	0.252
Surface area /m^2/g	
DeLaunay diameter /Å	4.00

Figure S9. Structural details for LTA-5A zeolite.

LTA-4A

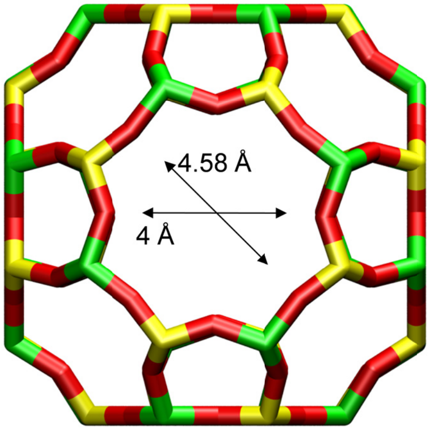

LTA-4A

The window dimension calculated using the van der Waals diameter of framework atoms = 2.7 Å is indicated above by the arrow.

Note that the Na^+ ions partially block the windows and therefore the diffusivities in LTA-4A are significantly lower than that for LTA Si. These cannot be determined from MD.

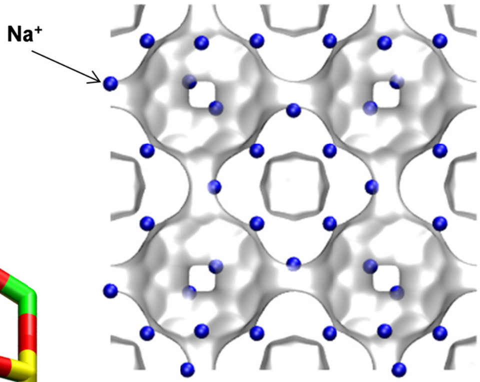

LTA-4A (96 Na+)

	LTA-4A
a /Å	24.555
b /Å	24.555
c /Å	24.555
Cell volume / $Å^3$	14805.39
conversion factor for [molec/uc] to [mol per kg Framework]	0.0733
conversion factor for [molec/uc] to [$kmol/m^3$]	0.2991
ρ [kg/m3] (with cations)	1529.55
MW unit cell [g/mol(framework+cations)]	13637.27
ϕ, fractional pore volume	0.375
open space / $Å^3$/uc	5552.0
Pore volume / cm^3/g	0.245
Surface area /m^2/g	
DeLaunay diameter /Å	4.00

Figure S10. Structural details for LTA-4A zeolite.

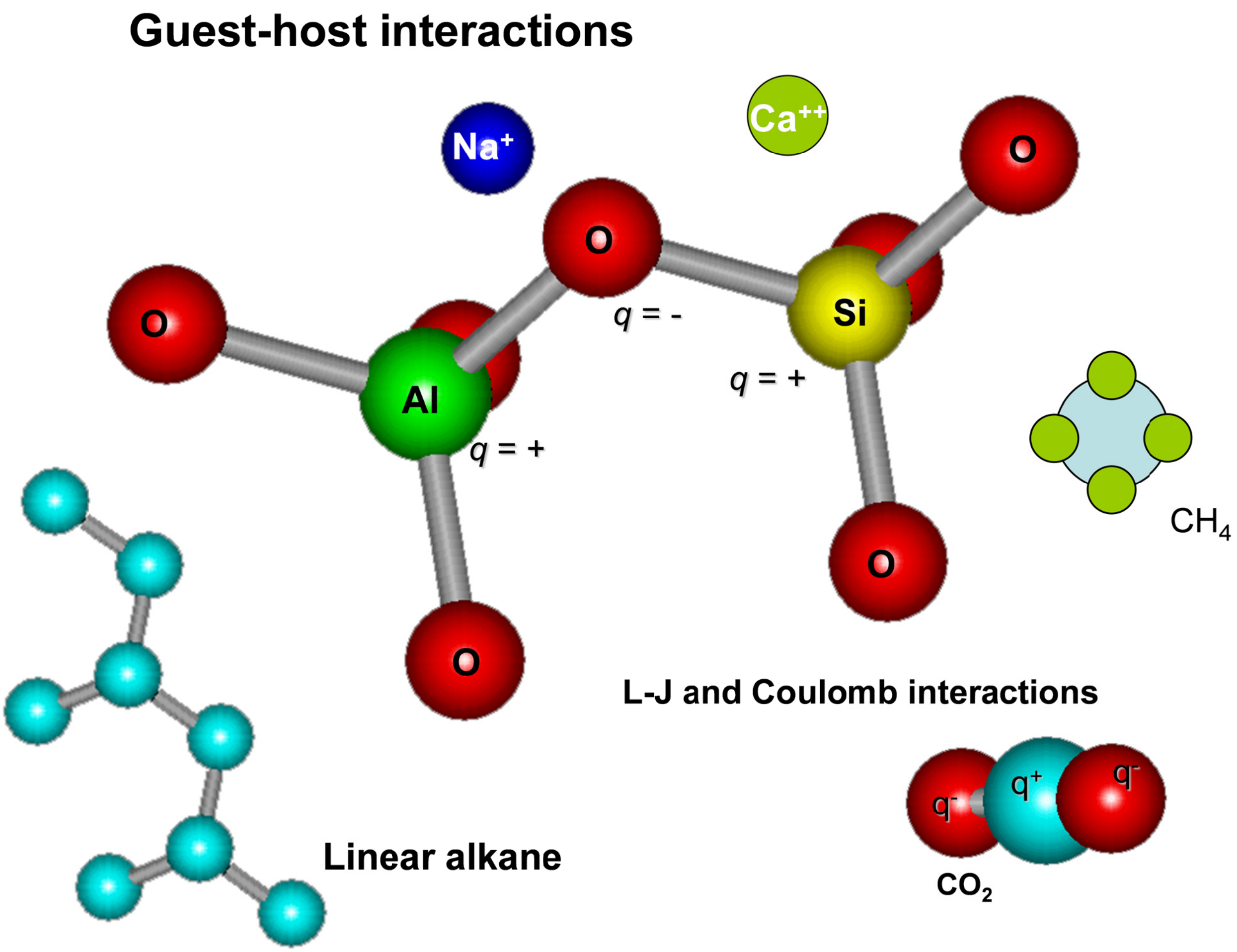

Figure S11. Guest-host interactions.

3 IAST calculations of mixture adsorption

3.1 Brief outline of theory

Within microporous crystalline materials such as zeolites and metal-organic frameworks (MOFs), the guest molecules exist in the adsorbed phase. The Gibbs adsorption equation[12] in differential form is

$$Ad\pi = \sum_{i=1}^{n} q_i d\mu_i \tag{S1}$$

The quantity A is the surface area per kg of framework, with units of m^2 per kg of the framework of the crystalline material; q_i is the molar loading of component i in the adsorbed phase with units moles per kg of framework; μ_i is the molar chemical potential of component i. The spreading pressure π has the same units as surface tension, i.e. N m^{-1}.

The chemical potential of any component in the adsorbed phase, μ_i, equals that in the bulk fluid phase. If the partial fugacities in the bulk fluid phase are f_i, we have

$$d\mu_i = RTd\ln f_i \tag{S2}$$

where R is the gas constant (= 8.314 J mol^{-1} K^{-1}).

Briefly, the basic equation of Ideal Adsorbed Solution Theory (IAST) theory of Myers and Prausnitz[13] is the analogue of Raoult's law for vapor-liquid equilibrium, i.e.

$$f_i = P_i^0 x_i; \quad i = 1,2,...n \tag{S3}$$

where x_i is the mole fraction in the adsorbed phase

$$x_i = \frac{q_i}{q_1 + q_2 + ...q_n} \tag{S4}$$

and P_i^0 is the pressure for sorption of every component i, which yields the same spreading pressure, π for each of the pure components, as that for the mixture:

IAST calculations of mixture adsorption

$$\frac{\pi A}{RT}=\int_0^{P_1^0}\frac{q_1^0(f)}{f}df=\int_0^{P_2^0}\frac{q_2^0(f)}{f}df=\int_0^{P_3^0}\frac{q_3^0(f)}{f}df=... \tag{S5}$$

where $q_i^0(f)$ is the *pure* component adsorption isotherm. The units of $\frac{\pi A}{RT}$, also called the adsorption potential,[14] are mol kg^{-1}.

The unary isotherm may be described by say the 1-site Langmuir isotherm

$$q^0(f)=q_{sat}\frac{bf}{1+bf};\quad \theta=\frac{bf}{1+bf} \tag{S6}$$

where we define the fractional *occupancy* of the adsorbate molecules, $\theta=q^0(f)/q_{sat}$. The superscript 0 is used to emphasize that $q^0(f)$ relates the *pure component* loading to the bulk fluid fugacity. More generally, the unary isotherms may need to be described by, say, the dual-site Langmuir-Freundlich model

$$q^0(f)=q_{A,sat}\frac{b_Af^{\nu_A}}{1+b_Af^{\nu_A}}+q_{B,sat}\frac{b_Bf^{\nu_B}}{1+b_Bf^{\nu_B}} \tag{S7}$$

Each of the integrals in Equation (S5) can be evaluated analytically:

$$\begin{aligned}\int_{f=0}^{P_i^0}\frac{q^0(f)}{f}df&=\frac{q_{A,sat}}{\nu_A}\ln\left(1+b_A\left(P_i^0\right)^{\nu_A}\right)+\frac{q_{B,sat}}{\nu_B}\ln\left(1+b_B\left(P_i^0\right)^{\nu_B}\right)\\ \int_{f=0}^{P_i^0}\frac{q^0(f)}{f}df&=\frac{q_{A,sat}}{\nu_A}\ln\left(1+b_A\left(\frac{f_i}{x_i}\right)^{\nu_A}\right)+\frac{q_{B,sat}}{\nu_B}\ln\left(1+b_B\left(\frac{f_i}{x_i}\right)^{\nu_B}\right)\end{aligned} \tag{S8}$$

The right hand side of eq (S8) is a function of P_i^0. For multicomponent mixture adsorption, each of the equalities on the right hand side of eq (S5) must be satisfied. These constraints may be solved using a suitable equation solver, to yield the set of values of P_1^0, P_2^0, P_3^0,.. P_n^0, all of which satisfy eq (S5). The corresponding values of the integrals using these as upper limits of integration must yield the same value of $\frac{\pi A}{RT}$ for each component; this ensures that the obtained solution is the correct one.

The adsorbed phase mole fractions x_i are then determined from

IAST calculations of mixture adsorption

$$x_i = \frac{f_i}{P_i^0}; \quad i = 1,2,...n \tag{S9}$$

A key assumption of the IAST is that the enthalpies and surface areas of the adsorbed molecules do not change upon mixing. If the total mixture loading is q_t, the area covered by the adsorbed mixture is $\frac{A}{q_t}$ with units of m^2 (mol mixture)$^{-1}$. Therefore, the assumption of no surface area change due to mixture adsorption translates as $\frac{A}{q_t} = \frac{Ax_1}{q_1^0\left(P_1^0\right)} + \frac{Ax_2}{q_2^0\left(P_2^0\right)} + \cdots \frac{Ax_n}{q_n^0\left(P_n^0\right)}$; the total mixture loading is q_t is calculated from

$$q_t = q_1 + q_2 ... + q_n = \frac{1}{\frac{x_1}{q_1^0(P_1^0)} + \frac{x_2}{q_2^0(P_2^0)} + ... + \frac{x_n}{q_n^0(P_n^0)}} \tag{S10}$$

in which $q_1^0(P_1^0)$, $q_2^0(P_2^0)$,… $q_n^0(P_n^0)$ are determined from the unary isotherm fits, using the sorption pressures for each component P_1^0, P_2^0, P_3^0,.. P_n^0 that are available from the solutions to Equations (S5), and (S8).

The entire set of equations (S3) to (S10) need to be solved numerically to obtain the loadings, q_i of the individual components in the mixture.

4 The Real Adsorbed Solution Theory (RAST)

To account for non-ideality effects in mixture adsorption, we introduce activity coefficients γ_i into Equation (S3) [13]

$$f_i = P_i^0 x_i \gamma_i \tag{S11}$$

Following the approaches of Myers, Talu, and Sieperstein[14-16] we model the excess Gibbs free energy for binary mixture adsorption as follows

$$\frac{G^{excess}}{RT} = x_1 \ln(\gamma_1) + x_2 \ln(\gamma_2) \tag{S12}$$

The Wilson model for activity coefficients are given for binary mixtures by

$$\begin{aligned}
\ln(\gamma_1) &= \left(1 - \ln(x_1\Lambda_{11} + x_2\Lambda_{12}) - \frac{x_1\Lambda_{11}}{x_1\Lambda_{11} + x_2\Lambda_{12}} - \frac{x_2\Lambda_{21}}{x_2 + x_1\Lambda_{21}}\right)\left(1 - \exp\left(-C\frac{\pi A}{RT}\right)\right) \\
\ln(\gamma_2) &= \left(1 - \ln(x_1\Lambda_{21} + x_2\Lambda_{22}) - \frac{x_1\Lambda_{12}}{x_1\Lambda_{11} + x_2\Lambda_{12}} - \frac{x_2\Lambda_{22}}{x_1\Lambda_{21} + x_2\Lambda_{22}}\right)\left(1 - \exp\left(-C\frac{\pi A}{RT}\right)\right)
\end{aligned} \tag{S13}$$

In Equation (S13), $\Lambda_{11} \equiv 1; \quad \Lambda_{22} \equiv 1$, and C is a constant with the units kg mol^{-1}. The introduction of $\left(1 - \exp\left(-C\frac{\pi A}{RT}\right)\right)$ imparts the correct limiting behaviors $\gamma_i \to 1; \quad \frac{\pi A}{RT} \to 0$ for the activity coefficients in the Henry regime, $f_t \to 0; \quad \frac{\pi A}{RT} \to 0$. As pore saturation conditions are approached, this correction factor tends to unity $\left(1 - \exp\left(-C\frac{\pi A}{RT}\right)\right) \to 1$. The choice of $\Lambda_{12} = \Lambda_{21} = 1$ in Equation (S13), yields unity values for the activity coefficients.

The excess reciprocal loading for the mixture can be defined as

$$\left(\frac{1}{q_t}\right)^{excess} = \frac{1}{q_t} - \left(\frac{x_1}{q_1^0(P_1^0)} + \frac{x_2}{q_2^0(P_2^0)}\right) \tag{S14}$$

The excess reciprocal loading for the mixture can be related to the partial derivative of the Gibbs free energy with respect to the adsorption potential at constant composition

The Real Adsorbed Solution Theory (RAST)

$$\left(\frac{1}{q_t}\right)^{excess} = \left.\frac{\partial\left(\frac{G^{excess}}{RT}\right)}{\partial\left(\frac{\pi A}{RT}\right)}\right|_{T,x} = \left[-x_1\ln(x_1 + x_2\Lambda_{12}) - x_2\ln\left(x_2 + x_1\Lambda_{21}\right)\right]C\exp\left(-C\frac{\pi A}{RT}\right) \tag{S15}$$

For calculation of the total mixture loading we need to replace Equation (S10) by

$$q_t \equiv q_1 + q_2 = \frac{1}{\frac{x_1}{q_1^0(P_1^0)} + \frac{x_2}{q_2^0(P_2^0)} + \left[-x_1\ln(x_1 + x_2\Lambda_{12}) - x_2\ln\left(x_2 + x_1\Lambda_{21}\right)\right]C\exp\left(-C\frac{\pi A}{RT}\right)} \tag{S16}$$

The parameters Λ_{12}, Λ_{21}, and C can be fitted to match the experimental data on mixture adsorption. The implementation of the activity coefficients is termed as the Real Adsorbed Solution Theory (RAST).

5 Binary mixture adsorption in zeolites

5.1 CO_2/CH_4 mixture adsorption in 13X zeolite; Gholipour experiments

Gholipour and Mofarahi[17] report the results of a comprehensive experimental investigation of adsorption equilibrium of CO_2/CH_4 mixture adsorption in 13X zeolite at pressures of 0.4 MPa and 0.6 MPa, and varying compositions of the bulk gas mixture. We present a re-analysis of their binary experimental data at 303 K as presented in Table 4 of their paper. Figure S12a presents a plot of the adsorbed phase mole fraction of CO_2 as a function of the mole fraction of CO_2 in the bulk gas mixture; the plotted data is for a total pressure of 0.6 MPa. The corresponding values of the CO_2/CH_4 adsorption selectivity are plotted in Figure S12b. As compared to the experimental data, the IAST severely overpredicts the selectivity values to a significant extent.

5.2 CO_2/CH_4 mixture adsorption in LTA-5A zeolite; Mofarahi experiments

Mofarahi and Gholipour[18] report the results of a comprehensive experimental investigation of adsorption equilibrium of describe CO_2/CH_4 mixture adsorption in LTA-5A zeolite at 303 K, 0.4 MPa, and varying compositions of the bulk gas mixture. We present a re-analysis of their binary experimental data as presented in Table 4, Table 9, and Table 11 of their paper. Figure S13a presents a plot of the adsorbed phase mole fraction of CO_2 as a function of the mole fraction of CO_2 in the bulk gas mixture; the plotted data is for 0.4 MPa total pressure. As compared to the experimental data, the IAST severely overpredicts the mole fraction of the adsorbed phase mole fraction of CO_2. The corresponding values of the CO_2/CH_4 adsorption selectivity are plotted in Figure S13b.

As compared to the experimental data, the IAST severely overpredicts the selectivity values to a significant extent.

5.3 CO_2/N_2 mixture adsorption in 13X zeolite; Hefti experiments

Hefti et al.[19] report the results of a comprehensive experimental investigation of adsorption equilibrium for CO_2/N_2 mixtures in ZSM-5 and 13X zeolites for pressures ranging to 1 MPa. As illustration, Figure S14a present experimental data (indicated by symbols) of Hefti et al.[19] for component loadings, q_i, of CO_2, and N_2 for adsorption of CO_2/N_2 mixtures in 13X zeolite at 298 K and total pressure p_t = 1 MPa, as function of the mole fraction of CO_2 in the bulk gas phase. The IAST (shown by the dashed lines) overestimates the CO_2 loading, and underestimates the N_2 loading; consequently the adsorption selectivities (see Figure S14b) are overly optimistic.

The overestimation of selectivities by IAST can be rationalized on the same basis as for CO_2/CH_4 separations with NaX zeolite, as discussed in the foregoing section. Due to strong coulombic interactions of CO_2 with the extra-framework Na^+ ions, the selectivity is strongly in favor of CO_2 There is a tendency of CO_2 molecules to congregate around the cations; this results in an inhomogeneous distribution of adsorbates CO_2 and N_2. The IAST calculation assumes that N_2 molecules compete with *all* of the CO_2, making no allowance for congregation of CO_2 around the cations. Due to congregation effects, the competition faced by N_2 molecules within the cages is *smaller* than that in the entire pore space. The IAST anticipates a stiffer competition between CO_2 and N_2 as it assumes a uniform distribution of composition; consequently, the separation selectivity is *over*estimated.

Use of the RAST model, shown by the continuous solid line, with fitted Wilson parameters Λ_{12} = 1.95; Λ_{21} = 64; C = 0.044 kg mol^{-1} in Figure S14a is able to model the congregation/segregation effects in mixture adsorption. The fitted Wilson parameters are based on the entire data set at 298 K, as reported in Section 2.2 of the Supplementary Material of Hefti et al.[19]

5.4 CO_2/N_2 mixture adsorption in 13X zeolite; Wilkins experiments

Figure S15a presents the unary isotherm data of CO_2, and N_2 in 13X zeolite at 298 K, as reported by in Table 1 and Table 2 of the Supplementary Material accompanying the publication of Wilkins and Rajendran.[20] The experimental CO_2 isotherms were fitted with a dual-Langmuir model; the experimental

N_2 isotherms were fitted with a 1-site-Langmuir model. The isotherm fit parameters are provided in Table S3. Figure S15b presents the experimental data (indicated by symbols) of Wilkins and Rajendran[20] for component loadings, q_i, of CO_2, and N_2 for adsorption of CO_2/N_2 mixtures in 13X zeolite at 296 K and total pressure $p_t =$ 97 kPa, as function of the mole fraction of CO_2 in the bulk gas phase, y_1. The dashed lines in Figure S15b are the IAST estimations using the unary isotherm fits provided in Table S3. The IAST estimations of the component loadings for N_2 are not in good agreement with the experimental data.

To match the experimental data on the component loadings, we need to introduce activity coefficients. Use of the RAST with fitted Wilson parameters $\Lambda_{12} = 8.5$; $\Lambda_{21} = 1$; $C = 0.025$ kg mol^{-1} results in a good match with the experiments. Figure S15c shows RAST calculations of the activity coefficients in the adsorbed phase. It is noteworthy that the activity coefficient of CO_2 is virtually unity over the entire composition range. On the other hand, the activity coefficient of N_2 shows increasing departure from unity as the mole fraction of CO_2 in the bulk gas phase, y_1, increases. Figure S15d plots the experimental data on the CO_2/N_2 adsorption selectivity as function of the mole fraction of CO_2 in the bulk gas phase. The IAST severely overestimates the adsorption selectivity.

5.5 CO_2/C_3H_8 mixture adsorption in NaX zeolite; Costa experiments

Costa et al.[21] report experimental data for adsorption of $CO_2(1)/C_3H_8(2)$ mixtures in NaX zeolite at 293 K. In Figure S16a, the adsorbed phase mole fraction of $CO_2(1)$, x_1, is plotted as function of mole fraction of $CO_2(1)$ in the bulk gas phase mixture, y_1. The experimental data clearly demonstrates the occurrence of the phenomenon of azeotropic adsorption, i.e. $x_1 = y_1$. The phenomenon of azeotropy is not anticipated by the IAST, as demonstrated the IAST calculations of adsorption selectivity S_{ads} for a total pressure of 50 kPa; see Figure S16b. The IAST is unable to anticipate the strong decrease in S_{ads} with increased mole fraction of $CO_2(1)$ in the bulk gas phase mixture, y_1; these characteristics are in line with the CBMC simulation data presented in Figure S24b. It is noteworthy that for $y_1 \approx 0.8$, we have mixture adsorption azeotropy, $x_1 = y_1; S_{ads} = 1$.

5.6 CO_2/N_2 mixture adsorption in NaX zeolite; CBMC simulations

Figure S17a presents CBMC simulations of unary isotherm data of CO_2, and N_2 in NaX (106 Si, 86 Al, 86 Na^+ with Si/Al=1.23) zeolite at 300 K. The CBMC CO_2 isotherms were fitted with a dual-Langmuir model; the CBMC N_2 isotherms were fitted with a 1-site-Langmuir model. The isotherm fit parameters are provided in Table S5. Figure S17b presents the CBMC simulation data (indicated by symbols) of component loadings, q_i, of CO_2, and N_2 for adsorption of CO_2/N_2 mixtures in NaX zeolite at 300K and total fugacity f_t = 100 kPa, as function of the mole fraction of CO_2 in the bulk gas phase, y_1. The dashed lines in Figure S17b are the IAST estimations using the unary isotherm fits provided in Table S5. The IAST estimations of the component loadings for N_2 are not in good agreement with the CBMC mixture simulations.

To match the CBMC mixture simulation data on the component loadings, we need to introduce activity coefficients. Use of the RAST with fitted Wilson parameters $\Lambda_{12} = 8.6$; $\Lambda_{21} = 0.12$; $C = 0.025$ kg mol^{-1} results in a good match with the CBMC mixture data. Figure S17c shows RAST calculations of the activity coefficients in the adsorbed phase. It is noteworthy that the activity coefficient of CO_2 is virtually unity over the entire composition range. On the other hand, the activity coefficient of N_2 shows increasing departure from unity as the mole fraction of CO_2 in the bulk gas phase, y_1, increases. Figure S17d plots the CBMC data on the CO_2/N_2 adsorption selectivity as function of the mole fraction of CO_2 in the bulk gas phase. The IAST severely overestimates the adsorption selectivity.

The failure of the IAST is traceable to the non-uniform distribution of the guest molecules CO_2, and N_2 within the cages of NaX zeolite. To demonstrate this, the CBMC simulation data on the spatial locations of the guest molecules were sampled to determine the inter-molecular distances. By sampling a total of 10^6 simulation steps, the radial distribution function (RDF) were determined for CO_2-CO_2, CO_2-Na^+, and CO_2-N_2 separation distances. Figure S18a presents the RDF data for a total fugacity f_t =

100 kPa and y_1=0.05. The samples were taken up to a radial distance of 12 Å, but the *x*-axis has been truncated at 8 Å because only the first peaks are of interest in the discussions to follow. The plotted RDF data has been normalized such that the area under each of the curves is identical to one another (and equals 1000). If we compare the first peaks, it is noteworthy that the CO_2-CO_2, and CO_2-Na^+ pairs are close together; indicating that the major proportion of CO_2 congregates around the cations. A further point to note is that the CO_2-N_2 separation distance is significantly higher than the CO_2-CO_2 separation distance. This implies that the N_2 molecules face a less severe competitive adsorption with CO_2 than is anticipated by the IAST.

The primary reason for the congregation of CO_2 molecules is the presence of cations. In order to demonstrate this we also carried out CBMC simulations for adsorption of CO_2/N_2 mixtures in all-silica zeolite at a total fugacity f_t = 500 kPa and y_1=0.25 at 300 K. The RDF data on the distances between the molecular pairs CO_2-CO_2, CO_2-N_2, and N_2-N_2 are shown in Figure S18b. We note that the peaks occur at practically the same intermolecular distances. This indicates that there are no congregation effects and that the guest molecules are homogeneously distributed within the pore landscape. Such a homogeneous distribution of guest molecules fulfils the requirement of the IAST theory. Consequently, we should expect the IAST to provide a good quantitative description of CO_2/N_2 mixture adsorption in all-silica zeolite. To confirm this expectation, Figure S19a compares the CBMC simulated values of the adsorption selectivity for equimolar CO_2/N_2 mixtures in all-silica FAU with the corresponding IAST calculations using the CBMC simulated unary isotherm fits in Table S7. There is perfect agreement the two data sets. In sharp contrast, the IAST calculations severely over-predict the adsorption selectivity for equimolar CO_2/N_2 mixtures in NaX zeolite because the actual competition faced by N_2 is less severe due to congregation effects.

5.7 CO_2/CH_4 mixture adsorption in NaX zeolite; CBMC simulations

Figure S20a presents CBMC simulations of unary isotherm data of CO_2, and CH_4 in NaX zeolite at 300 K. The CBMC CO_2 isotherms were fitted with a dual-Langmuir model; the CBMC CH_4 isotherms were fitted with a 1-site-Langmuir model. The isotherm fit parameters are provided in Table S6. Figure S20b presents the CBMC simulation data (indicated by symbols) of component loadings, q_i, of CO_2, and CH_4 for adsorption of CO_2/CH_4 mixtures in NaX zeolite at 300K and total fugacity f_t = 100 kPa, as function of the mole fraction of CO_2 in the bulk gas phase, y_1. The dashed lines in Figure S20b are the IAST estimations using the unary isotherm fits provided in Table S6. The IAST estimations of the component loadings for CH_4 are not in good agreement with the CBMC mixture simulations.

To match the CBMC mixture simulation data on the component loadings, we need to introduce activity coefficients. Use of the RAST with fitted Wilson parameters $\Lambda_{12} = 1.35$; $\Lambda_{21} = 1.35$; $C = 1$ kg mol^{-1} results in a good match with the CBMC mixture data. Figure S20c shows RAST calculations of the activity coefficients in the adsorbed phase. It is noteworthy that the activity coefficient of CO_2 is virtually unity over the entire composition range. On the other hand, the activity coefficient of CH_4 shows increasing departure from unity as the mole fraction of CO_2 in the bulk gas phase, y_1, increases. Figure S20d plots the CBMC data on the CO_2/CH_4 adsorption selectivity as function of the mole fraction of CO_2 in the bulk gas phase. The IAST severely overestimates the adsorption selectivity.

The failure of the IAST is traceable to the non-uniform distribution of the guest molecules CO_2, and CH_4 within the cages of NaX zeolite. To demonstrate this, the CBMC simulation data on the spatial locations of the guest molecules were sampled to determine the inter-molecular distances. By sampling a total of 10^5 simulation steps, the radial distribution of the separation distances between the molecular pairs CO_2-CO_2, CO_2-Na^+, CO_2-CH_4, and CH_4-CH_4 were determined. The samples were taken upto a radial distance of 12 Å, but the *x*-axis has been truncated at 8 Å because only the first peaks are of interest in the discussions to follow. The plotted RDF data has been normalized such that the area under each of the curves is identical to one another (and equals 1000). Figure S21a presents the RDF data for a total fugacity f_t = 100 kPa and y_1=0.05. If we compare the first peaks, it is noteworthy that the CO_2-CO_2, and CO_2-Na^+ pairs are close together, indicating that the major proportion of CO_2 congregates around the cations. A further point to note is that the CO_2-CH_4 separation distance is significantly higher than the CO_2-CO_2 and CH_4-CH_4 separation distances. This implies that the CH_4 molecules face a less severe competitive adsorption with CO_2 than is anticipated by the IAST.

A visual appreciation of the congregation effects can be gained from the snapshot presented in Figure S22.

The primary reason for the congregation of CO_2 molecules is the presence of cations. In order to demonstrate this we also carried out CBMC simulations for adsorption of CO_2/CH_4 mixtures in all-silica zeolite at a total fugacity f_t = 500 kPa and y_1=0.25 at 300 K. The RDF data on the distances between the molecular pairs CO_2-CO_2, CO_2-CH_4, and CH_4-CH_4 are shown in Figure S21b. We note that the peaks occur at practically the same intermolecular distances. This indicates that there are no congregation effects and that the guest molecules are homogeneously distributed within the pore landscape. Such a homogeneous distribution of guest molecules fulfils the requirement of the IAST theory. Consequently, we should expect the IAST to provide a good quantitative description of CO_2/CH_4 mixture adsorption in all-silica zeolite. To confirm this expectation, Figure S23a compares the CBMC simulated values of the adsorption selectivity for equimolar CO_2/CH_4 mixtures in all-silica FAU with the corresponding IAST calculations using the CBMC simulated unary isotherm fits in Table S7. There is perfect agreement the two data sets. In sharp contrast, the IAST calculations severely over-predict the adsorption selectivity for equimolar CO_2/CH_4 mixtures in NaX zeolite because the actual competition faced by CH_4 is less severe due to congregation effects.

5.8 CO_2/C_3H_8 mixture adsorption in NaX zeolite

Figure S24a presents CBMC simulations of unary isotherm data of CO_2, and C_3H_8 in NaX zeolite at 300 K. The CBMC CO_2 isotherms were fitted with a dual-Langmuir model; the CBMC C_3H_8 isotherms were fitted with a 1-site-Langmuir model. The isotherm fit parameters are provided in Table S6. Figure S24b presents the CBMC simulation data (indicated by symbols) of component loadings, q_i, of CO_2, and C_3H_8 for adsorption of CO_2/C_3H_8 mixtures in NaX zeolite at 300K and total fugacity f_t = 1 MPa, as function of the mole fraction of CO_2 in the bulk gas phase, y_1. The dashed lines in Figure S24b are the

IAST estimations using the unary isotherm fits provided in Table S5. The IAST estimations of the component loadings for both CO_2, and C_3H_8 are not in good agreement with the CBMC mixture simulations.

To match the CBMC mixture simulation data on the component loadings, we need to introduce activity coefficients. Use of the RAST with fitted Wilson parameters $\Lambda_{12} = 1.5$; $\Lambda_{21} = 2.4$; $C = 1$ kg mol^{-1} results in a good match with the CBMC mixture data. Figure S24c shows RAST calculations of the activity coefficients in the adsorbed phase. Figure S24d plots the CBMC data on the CO_2/C_3H_8 adsorption selectivity as function of the mole fraction of CO_2 in the bulk gas phase. The IAST overestimates the adsorption selectivity for a range of mole fractions $y_1 > 0.3$.

Figure S25b,c present the corresponding results for CBMC simulation data (indicated by symbols) of component loadings, q_i, of CO_2, and C_3H_8 for adsorption of CO_2/C_3H_8 mixtures in NaX zeolite at 300K and total fugacity $f_t = 50$ kPa, as function of the mole fraction of CO_2 in the bulk gas phase, y_1. In this case, the CBMC data shows selectivity reversal at $y_1 > 0.8$, in agreement with the experimental findings of Costa et al.[21] (cf. Figure S24b).

The failure of the IAST is traceable to the non-uniform distribution of the guest molecules CO_2, and C_3H_8 within the cages of NaX zeolite. The failure of the IAST to provide quantitatively accurate estimates of component loadings, and adsorption selectivities is attributable to the inhomogeneous distribution of adsorbates in the pore space of NaX zeolite, caused by strong binding of CO_2 with the extra-framework cations. The inhomogeneous distribution is clearly visualized by the computational snapshot in Figure S26 for $f_1 = 0.5$ MPa, and $f_2 = 0.5$ MPa. We note that the bottom cage contains only CO_2, and there is no C_3H_8 present in that cage. One of the key assumptions of the IAST is that the distribution of adsorbates within the pore space is homogenous.

To quantify the inhomogeneous distribution of adsorbates, the CBMC simulation data on the spatial locations of the guest molecules were sampled to determine the inter-molecular distances. By sampling a total of 10^7 simulation steps, the radial distribution of the separation distances between the molecular pairs CO_2-CO_2, CO_2-Na^+, CO_2-C_3H_8, and C_3H_8-C_3H_8 were determined. Figure S27 presents the RDF data for a total fugacity f_t = 1 MPa and y_1=0.5. The samples were taken up to a radial distance of 12 Å, but the *x*-axis has been truncated at 8 Å because only the first peaks are of interest in the discussions to follow. The plotted RDF data has been normalized such that the area under each of the curves is identical to one another (and equals 1000). If we compare the first peaks, it is noteworthy that the CO_2-CO_2, and CO_2-Na^+ pairs are close together, indicating that the major proportion of CO_2 congregates around the cations. A further point to note is that the CO_2-C_3H_8 separation distance is significantly higher than the CO_2-CO_2 and C_3H_8-C_3H_8 separation distances. This implies that the C_3H_8 molecules face a less severe competitive adsorption with CO_2 than is anticipated by the IAST.

Since the root cause of the failure of the IAST is the strong binding of CO_2 with the extra-framework cations, we should expect the non-ideality effects to be negligibly small in all-silica zeolites, with no extra-framework cations. In order to verify this, we performed CBMC simulations $CO_2(1)/C_3H_8(2)$ mixture adsorption in all-silica FAU zeolite at 300 K and total fugacity f_t = 1 MPa, with varying CO_2 in the bulk gas phase; the results are presented in Figure S28. As anticipated, the IAST estimates of component loadings, and adsorption selectivities are in good agreement with CBMC data.

5.9 CO_2/C_3H_8 mixture adsorption in LTA-4A zeolite

Two different campaigns were carried out for CBMC simulations of $CO_2(1)/C_3H_8(2)$ mixture adsorption in LTA-4A zeolite at 300 K:

(i) the mole fraction of $CO_2(1)$ in the bulk gas phase is held constant, y_1 = 0.1, and the bulk gas phase fugacity $f_t = f_1 + f_2$ was varied, and

(ii) the mole fraction of $CO_2(1)$ in the bulk gas phase, y_1 was varied from 0 to 1, keeping the bulk gas phase mixture fugacity $f_t = f_1 + f_2$ constant at a value of 1 MPa.

The results of these two separate campaigns are presented, respectively, in Figure S29, and Figure S30; these data sets are discussed in turn below.

For $f_t = f_1 + f_2 < 10^6$ Pa, the selectivity is in favor of C_3H_8; with increasing values of the bulk gas phase fugacity $f_t = f_1 + f_2 > 10^6$, the adsorption selectivity S_{ads} becomes increasingly in favor of CO_2, due to strong Coulombic interactions with the extra-framework cations Na^+; see Figure S29b. The IAST does not anticipate this selectivity reversal in favor of CO_2.

The CBMC simulations can be matched by quantification of thermodynamic non-idealities using the Wilson parameters as specified in Table S9. Figure S29c shows the RAST calculations of the activity coefficients as function of $\pi A/RT$.

The CBMC simulations for $CO_2(1)/C_3H_8(2)$ mixture adsorption at f_t = 1 MPa, and varying mole fractions of $CO_2(1)$ in the bulk gas phase, y_1, are shown in Figure S30. For $y_1 < 0.1$, $S_{ads} > 1$, and the selectivity is in favor of CO_2. The CBMC simulations show that the adsorption selectivity S_{ads} is increasingly lowered below unity, i.e. in favor of the alkane, with increasing proportion of $CO_2(1)$ in the bulk gas phase; see Figure S30b. The IAST anticipates S_{ads} to be virtually Figure S30c shows the RAST calculations of the activity coefficients as function of the mole fraction of $CO_2(1)$ in the adsorbed phase, x_1.

The rationale for the departures from IAST estimates can be traced to congregation of CO_2 near the Na^+ cations, as witnessed in the RDFs for various guest pairs CO_2-CO_2, CO_2-Na^+, CO_2-C_3H_8, and C_3H_8-C_3H_8 shown in Figure S31. It is noteworthy that the first peaks of CO_2-CO_2 and Na^+-Na^+ are close together. Also noteworthy is that the first peaks of CO_2-CO_2 and CO_2-C_3H_8 are farther apart, indicating segregation effects. Also noteworthy, is that a number of peaks occur for CO_2-CO_2 pairs; two of these peaks correspond to the window-to-window distances of 8.68, and 12.27 Å.

5.10 CO_2/CH_4 mixture adsorption in all-silica DDR zeolite

A key assumption of the IAST is that the composition of the adsorbed phase is homogeneously and uniformly distributed within zeolite or metal-organic frameworks. Preferential location of molecules at certain locations within the crystalline, causes segregated adsorption and deviations from the assumption of homogeneous distribution. For separation of CO_2 from gaseous mixtures with CH_4, cage-type zeolites such as CHA, DDR, LTA, and ERI are of practical interest; these materials consist of cages separated by narrow windows, in the 3.3 – 4.5 Å range. For adsorption of CO_2/CH_4 mixtures, CBMC simulations[22] show that the window regions of cage-type zeolites has a significantly higher proportion of CO_2 than within the cages; see computational snapshots in Figure S32

For all four zeolites, the IAST under-predicts the loading of the more weakly adsorbed CH_4 in the CO_2/CH_4 mixture.[22, 23] The conventional IAST calculation assumes that CH_4 molecules compete with *all* of the CO_2, making no allowance for segregation. Due to segregation effects the competition faced by CH_4 molecules within the cages, where they almost exclusively reside, is *smaller* than that in the entire pore space. The IAST anticipates a stiffer competition between CO_2 and CH_4 as it assumes a uniform distribution of composition; consequently, the separation selectivity is *over*estimated. Due to the segregated nature of mixture adsorption, the IAST is unable to predict the mixture loadings accurately. Due to preferential location of CO_2 in the window regions the CH_4 molecules experience a less severe competition from CO_2. Figure S32 illustrate the segregation effects in DDR.

Figure S32b shows CBMC simulation data[22] of adsorption selectivity, S_{ads}, for $CO_2(1)/CH_4(2)$ mixtures in DDR zeolite at 300 K; the total bulk gas mixture fugacity is held constant, $f_t = f_1 + f_2 = 10^6$ Pa, and S_{ads} is plotted as a function of the bulk gas mixture of $CO_2(1)$, y_1. The IAST calculations do not predict the right trends in the dependence of S_{ads} on y_1. In Figure S32c, both sets of data plotted as function of the adsorption potential $\pi A/RT$. It is noteworthy, that the CBMC simulated data are not uniquely determined by the adsorption potential, $\pi A/RT$, because the thermodynamic non-ideality effects are non-negligible.

The two sets of CBMC data are adequately captured by the choice of the Wilson parameters $\Lambda_{12} = 0.81;\quad \Lambda_{21} = 3;\quad C = 0.34 \text{ mol kg}^{-1}$, as evidenced by the RAST calculations indicated by the continuous solid lines in Figure S32a,b,c. Figure S32d presents the calculations of the activity coefficients of the components, plotted as a function of the adsorption potential $\pi A/RT$. It is noteworthy that the non-idealities affect the activity coefficient of CH_4, but not that of CO_2.

The rationale for the departures from IAST estimates can be traced to congregation of CO_2 near the Na^+ cations, as witnessed in the RDFs for various guest pairs CO_2-CO_2, CO_2-CH_4, and CH_4-CH_4 shown in Figure S33. It is noteworthy that the first peaks of CO_2-CO_2 and CO_2-CH_4 are farther apart, indicating segregation effects. Also noteworthy is that the second peak for CO_2-CO_2 pairs corresponds to the window-to-window distance of 6.93 Å, indicating perching of CO_2 at the window regions.

5.11 List of Tables for Binary mixture adsorption in zeolites

Table S1. Dual-site Langmuir parameters for pure components CO_2, and CH_4 at 303 K in 13X zeolite. These parameters are based on the unary isotherm data reported in Figure 2 and Figure 3 of Gholipour and Mofarahi.[17]

	Site A		Site B	
	$q_{A,sat}$ mol kg^{-1}	b_A Pa^{-1}	$q_{B,sat}$ mol kg^{-1}	b_B Pa^{-1}
CO_2	3.1	9.38×10^{-6}	2.5	4.4×10^{-4}
CH_4	6.7	7.64×10^{-7}		

Table S2. Dual-site Langmuir parameters for pure components CO_2, and CH_4 at 303 K in LTA-5A zeolite. These parameters are based on the unary isotherm data reported in Figure 2 and Figure 3 of Mofarahi and Gholipour.[18]

	Site A		Site B	
	$q_{A,sat}$ mol kg^{-1}	b_A Pa^{-1}	$q_{B,sat}$ mol kg^{-1}	b_B Pa^{-1}
CO_2	1.4	7.33×10^{-6}	2.5	7.32×10^{-4}
CH_4	3.2	1.74×10^{-6}		

Table S3. Dual-site Langmuir parameters for pure components CO_2, and N_2 at 298 K in 13X zeolite. These fits are based on the 298 K unary isotherm data in Table 1 and Table 2 of the Supplementary Material accompanying the publication of Wilkins and Rajendran.[20]

	Site A		Site B	
	$q_{A,sat}$ mol kg^{-1}	b_A Pa^{-1}	$q_{B,sat}$ mol kg^{-1}	b_B Pa^{-1}
CO_2	3.8	1.16×10^{-4}	1.8	1.04×10^{-2}
N_2	4.0	1.1×10^{-6}		

Fitted Wilson non-ideality parameters for binary CO_2/N_2 mixture adsorption in 13X.

	Λ_{12}	Λ_{21}	C / kg mol^{-1}
CO_2/N_2 in 13X	8.5	1	0.025

Table S4. Dual-site Langmuir parameters for pure components CO_2, and C_3H_8 at 293 K in 13X (= NaX) zeolite. The fit parameters were determined by fitting the unary isotherm data presented in Table I of Costa et al.[21]

	Site A		Site B	
	$q_{A,sat}$ mol kg^{-1}	b_A Pa^{-1}	$q_{B,sat}$ mol kg^{-1}	b_B Pa^{-1}
CO_2	2.2	6.7×10^{-4}	2.5	3.47×10^{-5}
C_3H_8	2.2	7.04×10^{-4}		

Wilson non-ideality parameters for binary mixtures at 293 K in NaX zeolite. These are determined by fitting to the experimental data of Costa et al.[21] as reported in their paper.

	Λ_{12}	Λ_{21}	C / kg mol^{-1}
CO_2/C_3H_8 in NaX	2	1.8	0.2

Table S5. Dual-site Langmuir parameters for pure components CO_2, and N_2 at 300 K in NaX zeolite containing 86 Na^+/uc with Si/Al=1.23. The fit parameters are based on the CBMC simulations of pure component isotherms.

	Site A		Site B	
	$q_{A,sat}$ mol kg^{-1}	b_A Pa^{-1}	$q_{B,sat}$ mol kg^{-1}	b_B Pa^{-1}
CO_2	1.7	1.39×10^{-5}	4.2	4.78×10^{-4}
N_2	2.85	1.93×10^{-7}		

Fitted Wilson non-ideality parameters for binary CO_2/N_2 mixture adsorption in NaX at 300 K.

	Λ_{12}	Λ_{21}	C / kg mol^{-1}
CO_2/N_2 in NaX (86 Na/uc)	8.6	0.12	0.025

Table S6. Dual-site Langmuir parameters for pure components CO_2, and CH_4 at 300 K in NaX zeolite containing 86 Na^+/uc with Si/Al=1.23. The fit parameters are based on the CBMC simulations of pure component isotherms.

	Site A		Site B	
	$q_{A,sat}$ mol kg^{-1}	b_A Pa^{-1}	$q_{B,sat}$ mol kg^{-1}	b_B Pa^{-1}
CO_2	1.7	1.39×10^{-5}	4.2	4.78×10^{-4}
CH_4	5.8	2.07×10^{-6}		

Fitted Wilson non-ideality parameters for binary CO_2/CH_4 mixture adsorption in NaX at 300 K.

	Λ_{12}	Λ_{21}	C / kg mol^{-1}
CO_2/CH_4 in NaX (86 Na/uc) at 300 K	1.35	1.35	1

Table S7. Dual-site Langmuir-Freundlich parameters for pure components CO_2, CH_4, and N_2 and C_3H_8 at 300K in all-silica FAU. The fit parameters are based on the CBMC simulations of pure component isotherms presented in earlier works.[1, 24, 25]

	Site A			Site B		
	$q_{\mathrm{A,sat}}$ mol kg^{-1}	b_{A} $\mathrm{Pa}^{-\nu_A}$	ν_{A} dimensionless	$q_{\mathrm{B,sat}}$ mol kg^{-1}	b_{B} $\mathrm{Pa}^{-\nu_B}$	ν_{B} dimensionless
CO_2	2.4	2.52×10^{-14}	2.4	6.7	6.74×10^{-7}	1
CH_4	4	7×10^{-9}	0.86	6.5	2.75×10^{-7}	1
N_2	5.2	1.55×10^{-9}	1	5.8	1.32×10^{-7}	1
C_3H_8	1.2	2.88×10^{-15}	3.4	2.6	1.51×10^{-5}	1

Table S8. Dual-site Langmuir parameters for pure components CO_2, and C_3H_8 at 300 K in NaX zeolite containing 86 Na^+/uc with Si/Al=1.23. The fit parameters are based on the CBMC simulations of pure component isotherms.

	Site A		Site B	
	$q_{A,sat}$ mol kg^{-1}	b_A Pa^{-1}	$q_{B,sat}$ mol kg^{-1}	b_B Pa^{-1}
CO_2	1.7	1.39×10^{-5}	4.2	4.78×10^{-4}
C_3H_8	3.1	8.91×10^{-4}		

Fitted Wilson non-ideality parameters for binary CO_2/C_3H_8 mixture adsorption in NaX at 300 K.

	Λ_{12}	Λ_{21}	C / kg mol^{-1}
CO_2/C_3H_8 in NaX (86 Na/uc)	1.5	2.4	1.0

Table S9. Dual-site Langmuir-Freundlich parameters for pure components CO_2, and C_3H_8 at 300 K in LTA-4A zeolite (96 Si, 96 Al, 96 Na^+, Si/Al=1). The fit parameters are based on the CBMC simulations of pure component isotherms.

	Site A			Site B		
	$q_{A,sat}$ mol kg^{-1}	b_A $Pa^{-\nu_A}$	ν_A dimensionless	$q_{B,sat}$ mol kg^{-1}	b_B $Pa^{-\nu_B}$	ν_B dimensionless
CO_2	3.1	4.13×10^{-4}	1	1.7	2.095×10^{-7}	1
C_3H_8	2.5	2.21×10^{-2}	1	0.9	6.18×10^{-6}	1

Fitted Wilson non-ideality parameters for binary CO_2/C_3H_8 mixture adsorption in LTA-4A at 300 K.

	Λ_{12}	Λ_{21}	C / kg mol^{-1}
CO_2/C_3H_8 in LTA-4A at 300 K	1	5.65	0.1

Table S10. Dual-site Langmuir-Freundlich parameters for guest molecules in DDR (all-silica) at 300 K. To convert from molecules uc^{-1} to mol kg^{-1}, multiply by 0.069346435.

	Site A			Site B		
	$\Theta_{A,sat}$ molecules uc^{-1}	b_A $Pa^{-\nu_A}$	ν_A dimensionless	$\Theta_{B,sat}$ molecules uc^{-1}	b_B $Pa^{-\nu_A}$	ν_B dimensionless
CO_2	21.630528	2.32E-06	0.74	43.261056	5.89E-06	1
CH_4	23.0725632	3.46E-06	1	34.6088448	3.41E-06	0.65

Fitted Wilson non-ideality parameters for binary CO_2/CH_4 mixture adsorption in DDR at 300 K.

	Λ_{12}	Λ_{21}	C / kg mol^{-1}
CO_2/CH_4 in DDR	0.81	3	0.34

5.12 List of Figures for Binary mixture adsorption in zeolites

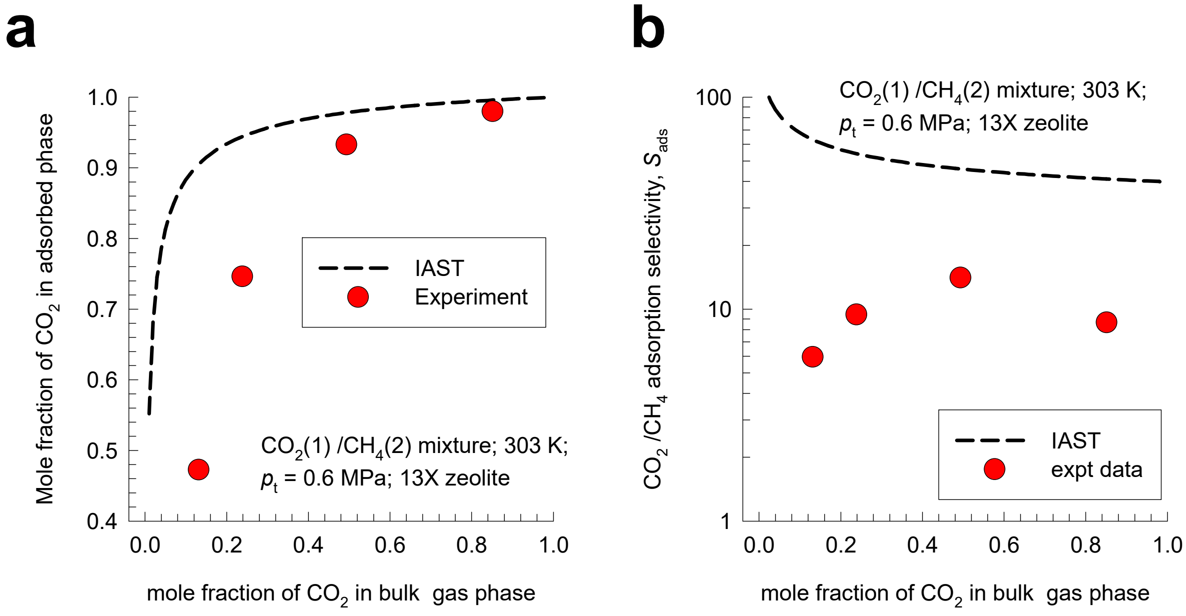

Figure S12. Re-analysis of the experimental data of Gholipour and Mofarahi[17] for CO_2(1)/CH_4(2) mixture adsorption at 303 K in 13X zeolite. (a) Experimental data (indicated by symbols) of adsorbed phase mole fractions, x_1, of CO_2, as function of the mole fraction of CO_2 in the bulk gas phase, y_1. (b) CO_2(1)/CH_4(2) adsorption selectivity as function of the mole fraction of CO_2 in the bulk gas phase. The dashed lines are the IAST estimations, using the unary isotherm fits, specified in Table S1.

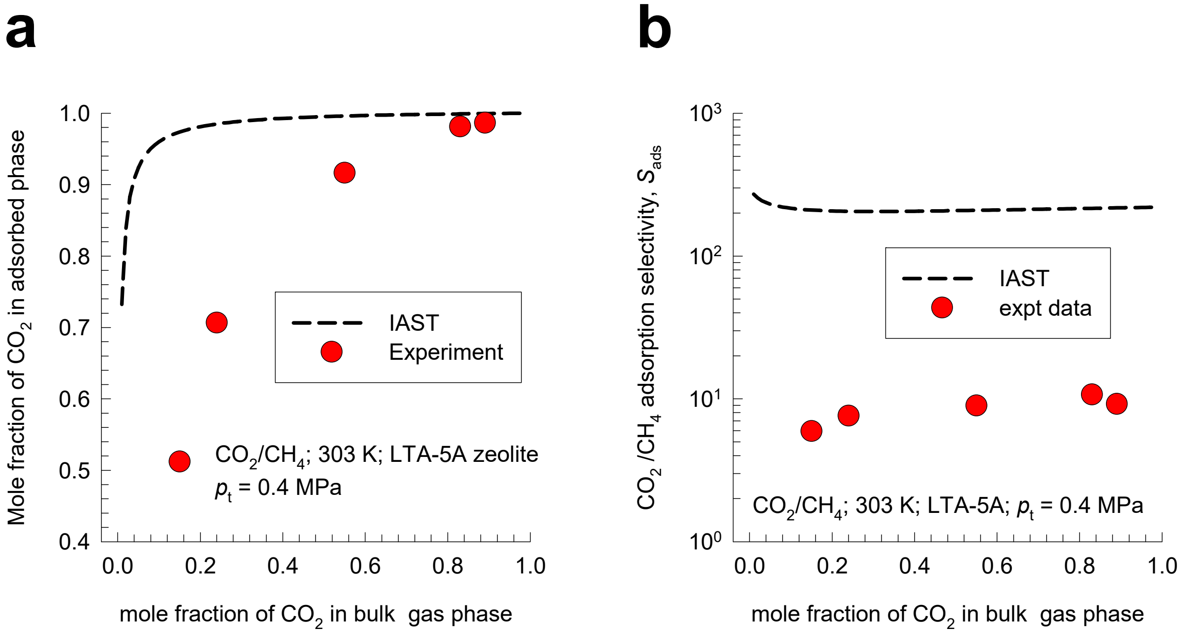

Figure S13 Re-analysis of the experimental data of Mofarahi and Gholipour[18] for $CO_2(1)/CH_4(2)$ mixture adsorption at 303 K in LTA-5A zeolite. (a) Experimental data (indicated by symbols) of adsorbed phase mole fractions, x_1, of CO_2, as function of the mole fraction of CO_2 in the bulk gas phase, y_1. (b) $CO_2(1)/CH_4(2)$ adsorption selectivity as function of the mole fraction of CO_2 in the bulk gas phase. The unary isotherm fit parameters are specified in Table S2.

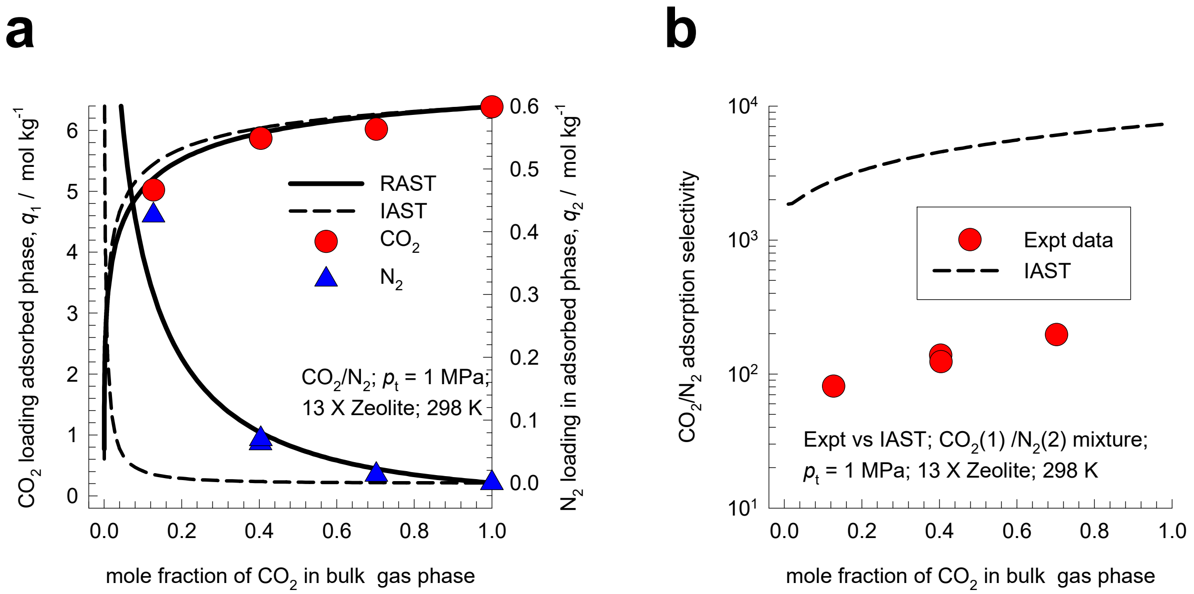

Figure S14. (a) Experimental data (indicated by symbols) of Hefti et al.[19] for component loadings, q_i, of CO_2, and N_2 for adsorption of CO_2/N_2 mixtures in 13X zeolite at 298 K and total pressure p_t = 1 MPa, as function of the mole fraction of CO_2 in the bulk gas phase. (b) CO_2/N_2 adsorption selectivity as function of the mole fraction of CO_2 in the bulk gas phase. The dashed lines in (a), and (b) are the IAST estimations, using the unary isotherm fits provided in Table 2 of Hefti et al.[19] The continuous solid lines in (a), and (b) are the estimations using RAST using Wilson parameters: $\Lambda_{12} = 1.95$; $\Lambda_{21} = 64$; $C = 0.044$ kg mol^{-1}.

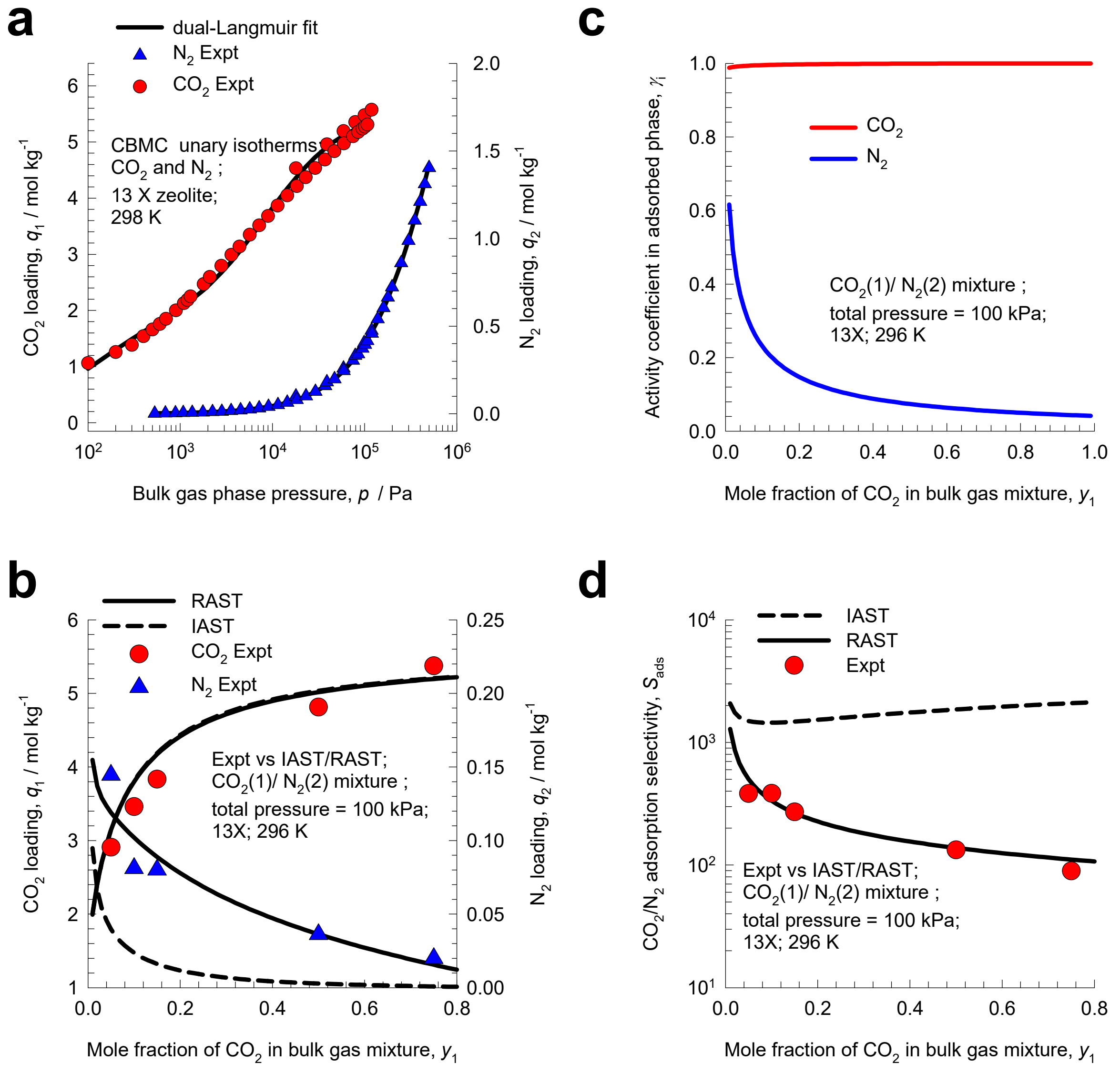

Figure S15. (a) Unary isotherm data of CO$_2$, and N$_2$ in 13X zeolite at 298 K. The isotherm fit parameters are provided in Table S3. (b) Experimental data (indicated by symbols) of Wilkins and Rajendran[20] for component loadings, q_i, of CO$_2$, and N$_2$ for adsorption of CO$_2$/N$_2$ mixtures in 13X zeolite at 296 K and total pressure p_t = 97 kPa, as function of the mole fraction of CO$_2$ in the bulk gas phase. (c) RAST calculations of the activity coefficients in the adsorbed phase. (d) CO$_2$/N$_2$ adsorption selectivity as function of the mole fraction of CO$_2$ in the bulk gas phase. The dashed lines in (b), and (d) are the IAST estimations, using the unary isotherm fits provided in Table S3. The continuous solid lines in (b), and (d) are the estimations using RAST using fitted Wilson parameters are provided in Table S3.

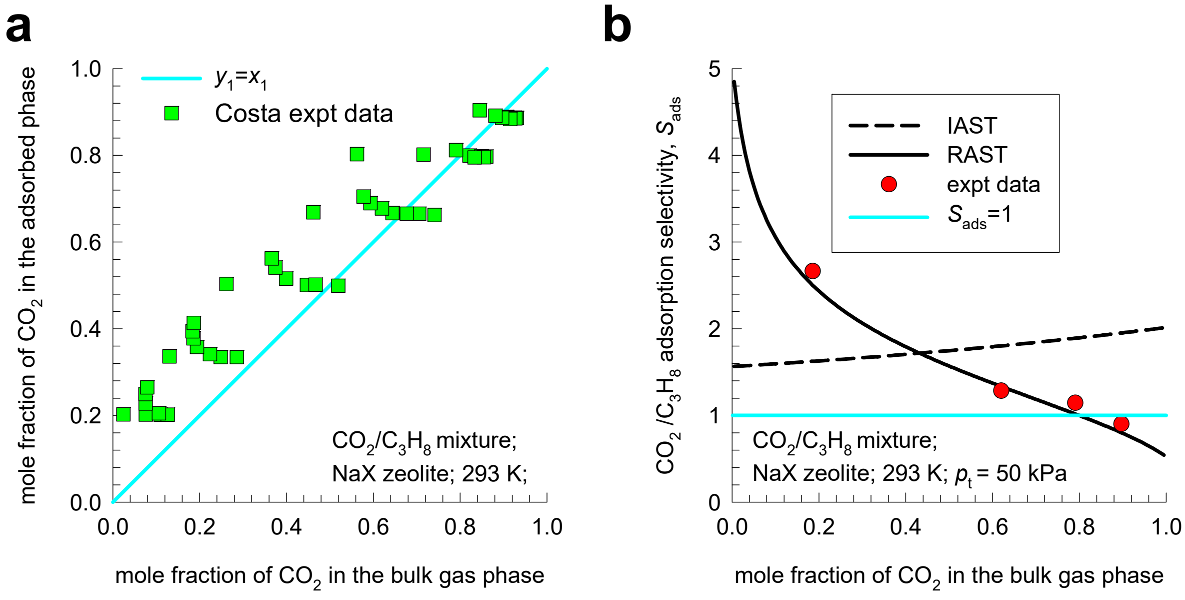

Figure S16. Re-analysis of the experimental data of Costa et al.[21] for adsorption of CO_2/C_3H_8 mixtures at 293 K in NaX (=13 X) zeolite. (a) Plot of the experimental data on mole fraction of CO_2 in the bulk gas phase, y_1, versus the mole fraction of CO_2 in the adsorbed phase, x_1. (b) The adsorption selectivity S_{ads} for $CO_2(1)/C_3H_8(2)$ mixture adsorption as a function of the mole fraction of CO_2 in the bulk gas phase, y_1. In this graph only data at total pressure = 50 kPa are plotted. Also shown in (b) are IAST (dashed lines) and RAST calculations (continuous solid lines) of S_{ads}. The unary isotherm fit parameters, along with the Wilson parameters, are specified in Table S4.

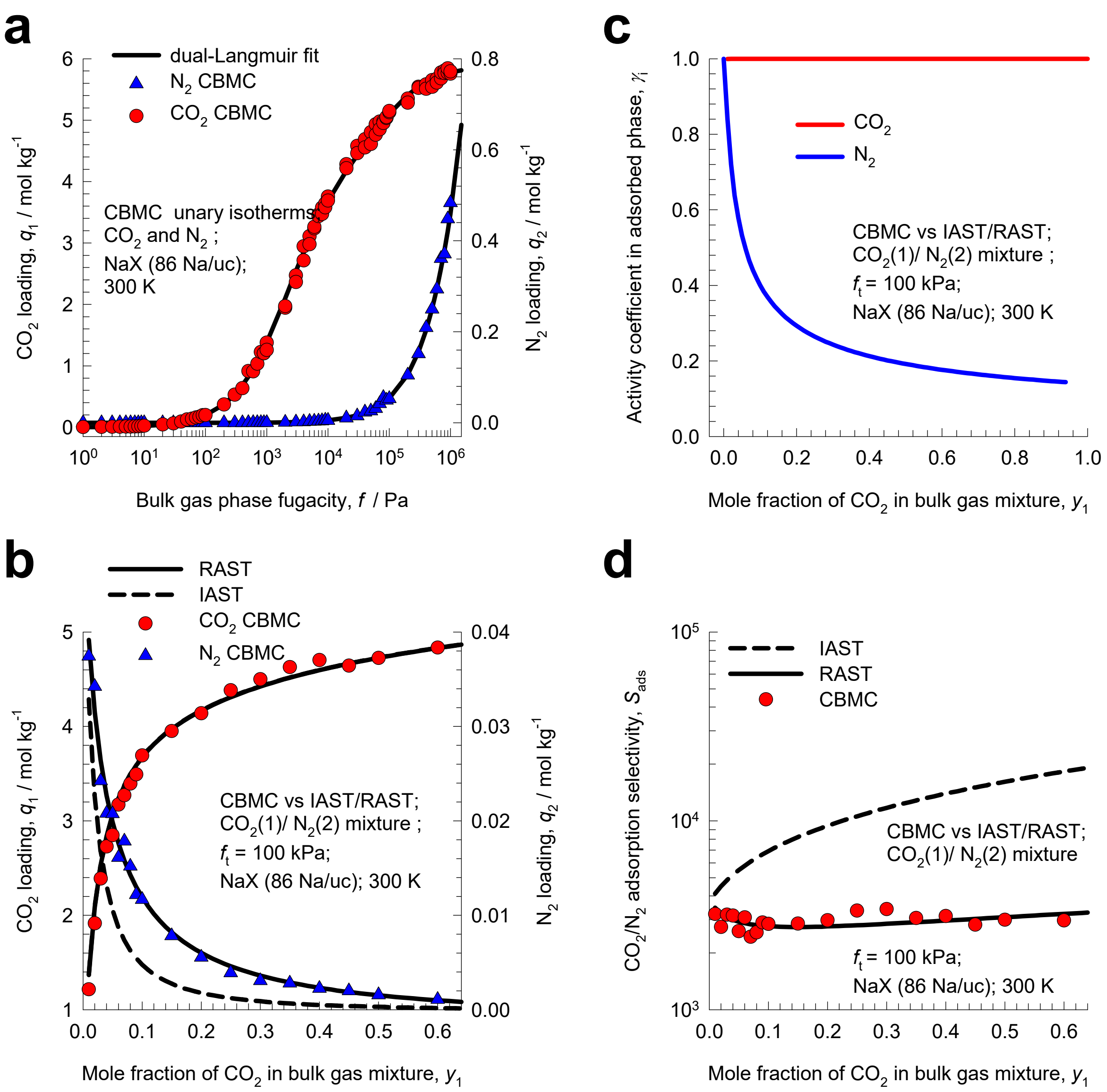

Figure S17. (a) CBMC simulations of unary isotherm data of CO_2, and N_2 in NaX zeolite at 300 K. The isotherm fit parameters are provided in Table S5. (b) CBMC simulation data (indicated by symbols) of for component loadings, q_i, of CO_2, and N_2 for adsorption of CO_2/N_2 mixtures in NaX zeolite at 300 K and total fugacity f_t = 100 kPa, as function of the mole fraction of CO_2 in the bulk gas phase, y_1. (c) RAST calculations of the activity coefficients in the adsorbed phase. (d) CO_2/N_2 adsorption selectivity as function of the mole fraction of CO_2 in the bulk gas phase. The dashed lines in (b), and (d) are the IAST estimations, using the unary isotherm fits. The continuous solid lines in (b), and (d) are the estimations using RAST using fitted Wilson parameters are provided Table S5.

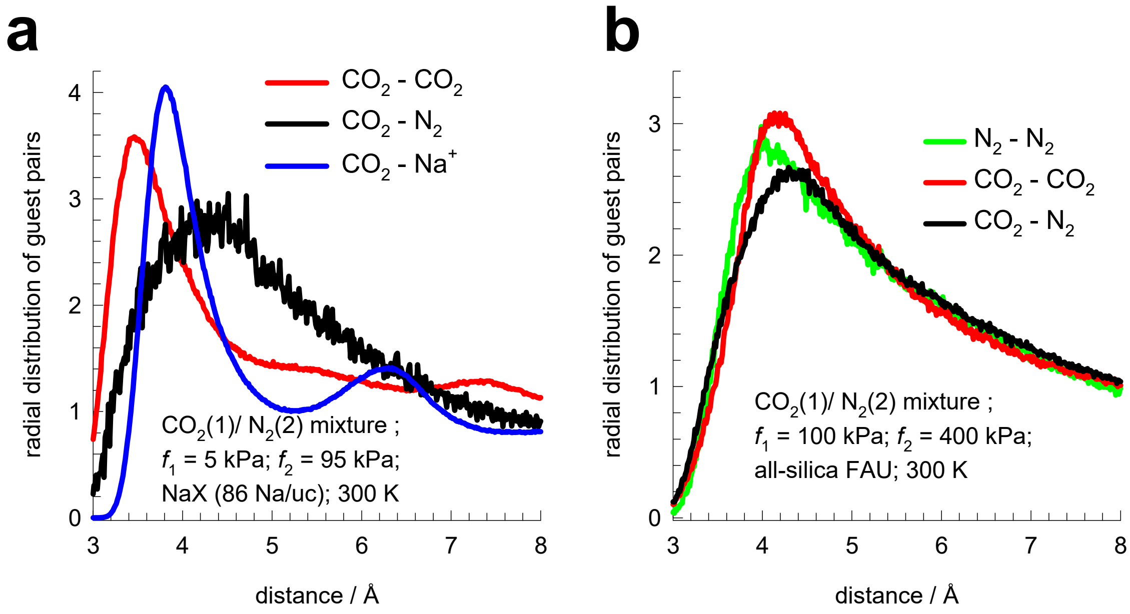

Figure S18. (a) Radial distribution of guest pairs determined from CBMC simulations for adsorption of CO_2/N_2 mixtures in NaX zeolite at 300 K and total fugacity f_t = 100 kPa, and y_1=0.05. (b) Radial distribution of guest pairs determined from CBMC simulations for adsorption of CO_2/N_2 mixtures in all-silica FAU zeolite at 300 K and total fugacity f_t = 500 kPa, and y_1=0.25.

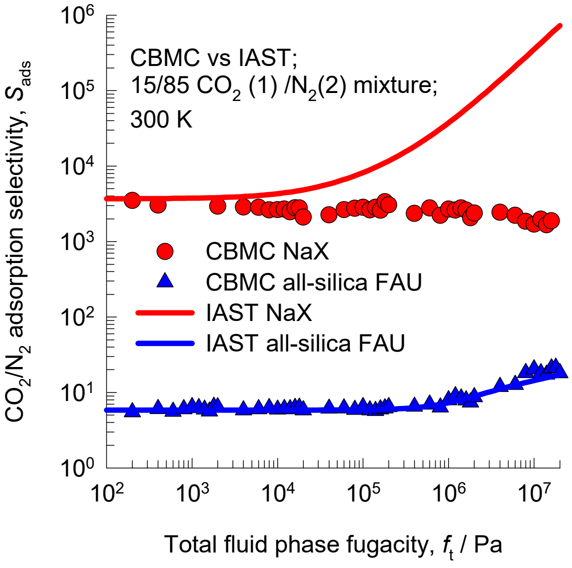

Figure S19. Comparison of CBMC simulated values of CO$_2$/N$_2$ adsorption selectivities determined from CBMC simulations for all-silica FAU (192 Si, 0 Al, 0 Na$^+$, Si/Al=∞), and NaX (106 Si, 86 Al, 86 Na$^+$, Si/Al=1.23) zeolites for equimolar mixtures at 300 K with IAST estimations. The unary isotherm parameters are provided in Table S7 (all-silica FAU), and Table S5 (NaX).

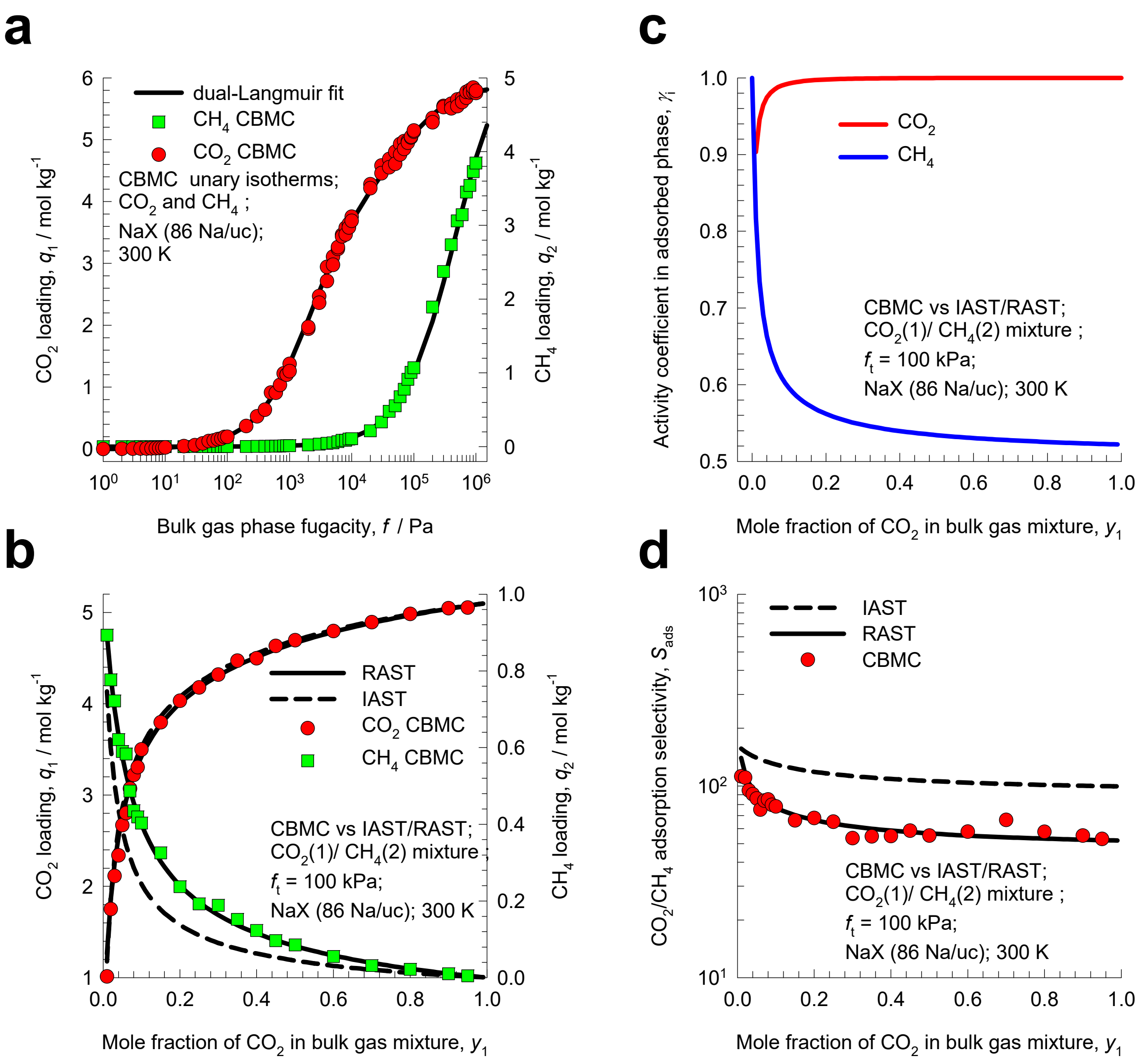

Figure S20. (a) CBMC simulations of unary isotherm data of CO$_2$, and CH$_4$ in NaX (106 Si, 86 Al, 86 Na$^+$, Si/Al=1.23) zeolite at 300 K. The isotherm fit parameters are provided in Table S6. (b) CBMC simulation data (indicated by symbols) of for component loadings, q_i, of CO$_2$, and CH$_4$ for adsorption of CO$_2$/ CH$_4$ mixtures in NaX zeolite at 300 K and total fugacity f_t = 100 kPa, as function of the mole fraction of CO$_2$ in the bulk gas phase, y_1. (c) RAST calculations of the activity coefficients in the adsorbed phase. (d) CO$_2$/CH$_4$ adsorption selectivity as function of the mole fraction of CO$_2$ in the bulk gas phase. The dashed lines in (b), and (d) are the IAST estimations. The continuous solid lines in (b), and (d) are the estimations using RAST using fitted Wilson parameters are provided in Table S6.

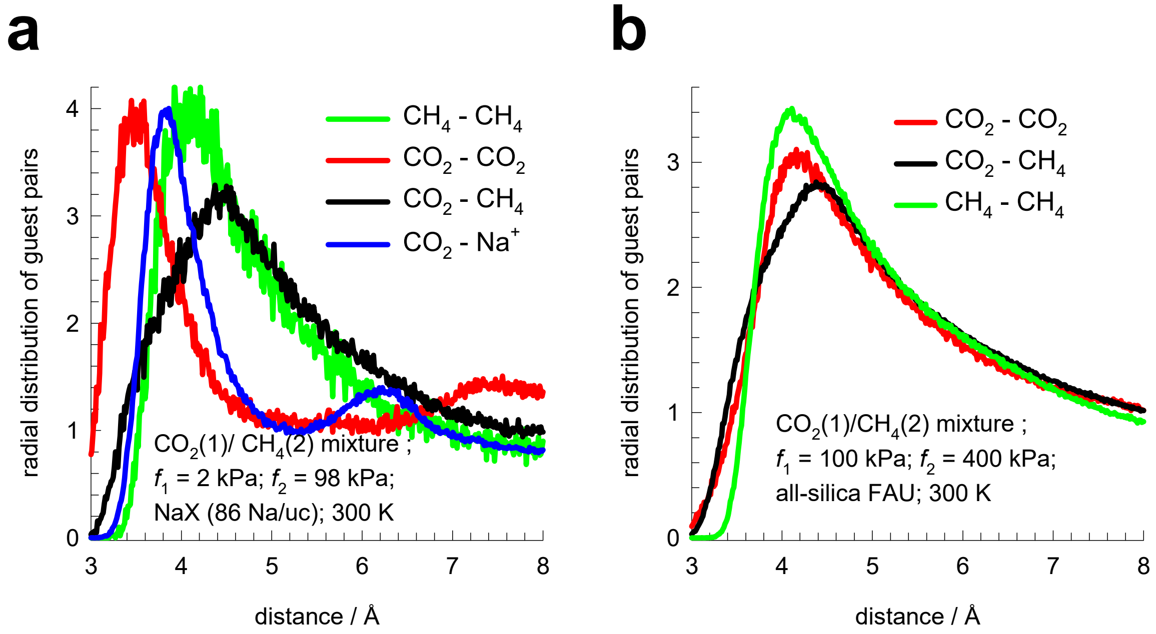

Figure S21. (a) Radial distribution of guest pairs determined from CBMC simulations for adsorption of CO_2/CH_4 mixtures in NaX zeolite at 300 K and total fugacity f_t = 100 kPa, and y_1=0.02. (b) Radial distribution of guest pairs determined from CBMC simulations for adsorption of CO_2/CH_4 mixtures in all-silica FAU zeolite at 300 K and total fugacity f_t = 500 kPa, and y_1=0.25.

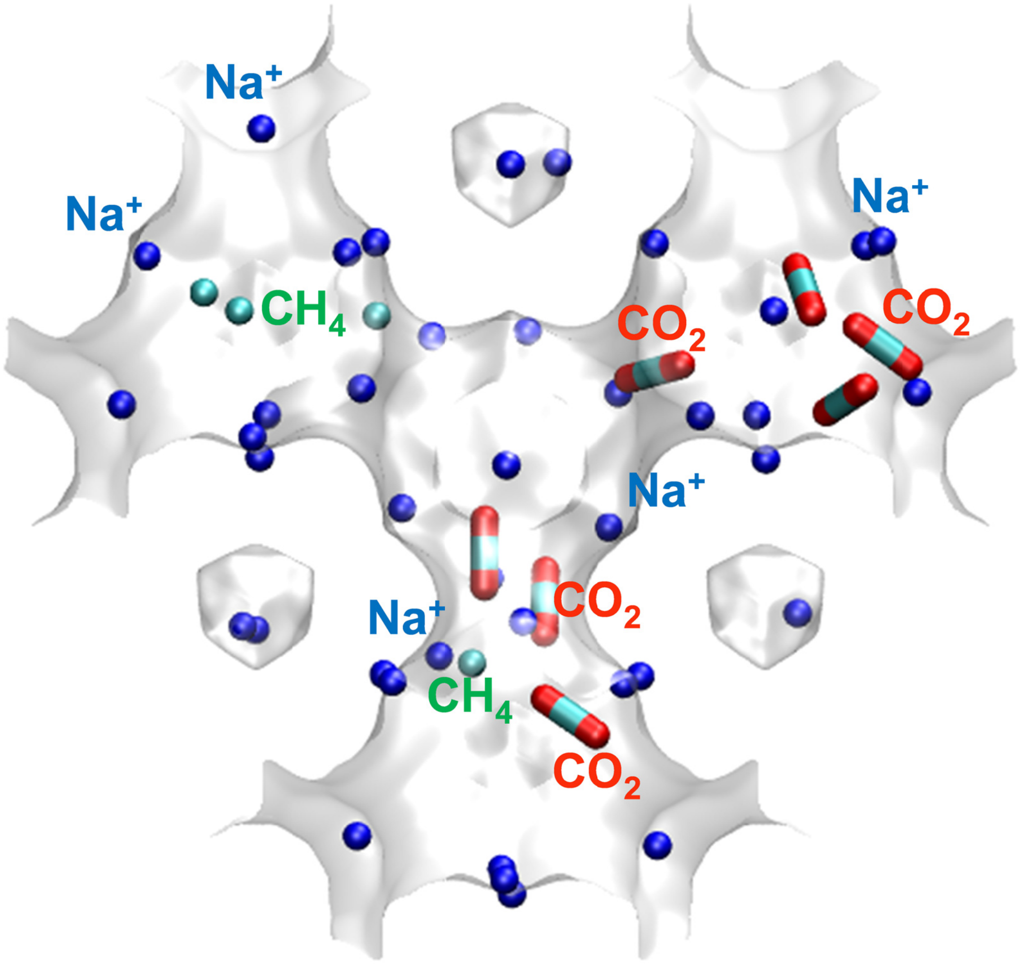

Figure S22. Snapshot showing the location of CO_2, CH_4, and Na+ cations within the pore landscape of NaX (106 Si, 86 Al, 86 Na^+, Si/Al=1.23) zeolite at 300 K and total fugacity f_t = 100 kPa, and y_1=0.02.

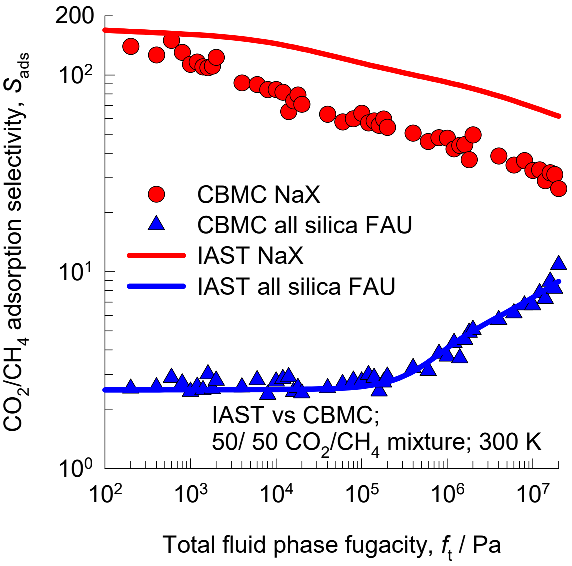

Figure S23. Comparison of CBMC simulated values of CO_2/CH_4 adsorption selectivities determined from CBMC simulations for all-silica FAU (192 Si, 0 Al, 0 Na^+, Si/Al=∞), and NaX (106 Si, 86 Al, 86 Na^+, Si/Al=1.23) zeolites for equimolar mixtures at 300 K with IAST estimations. The unary isotherm parameters are provided in Table S7 (all-silica FAU), and Table S6 (NaX).

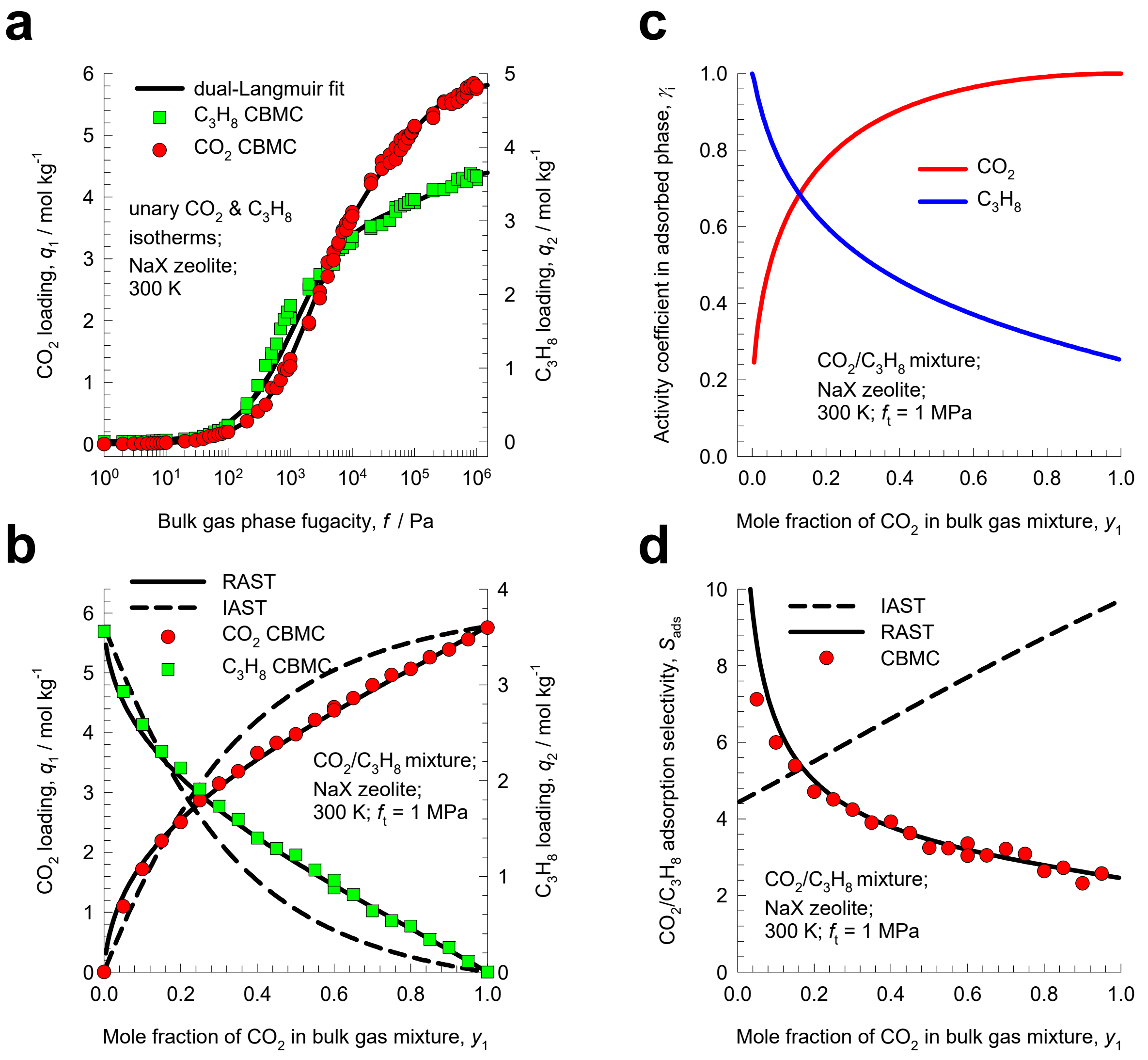

Figure S24. (a) CBMC simulations of unary isotherm data of CO_2, and C_3H_8 in NaX (106 Si, 86 Al, 86 Na^+, Si/Al=1.23) zeolite at 300 K. The isotherm fit parameters are provided in Table S8. (b) CBMC simulation data (indicated by symbols) of for component loadings, q_i, of CO_2, and C_3H_8 for adsorption of CO_2/C_3H_8 mixtures in NaX zeolite at 300 K and total fugacity f_t = 1 MPa, as function of the mole fraction of CO_2 in the bulk gas phase, y_1. (c) RAST calculations of the activity coefficients in the adsorbed phase. (d) CO_2/C_3H_8 adsorption selectivity as function of the mole fraction of CO_2 in the bulk gas phase. The dashed lines in (b), and (d) are the IAST estimations. The continuous solid lines in (b), and (d) are the estimations using RAST using fitted Wilson parameters are provided in Table S8.

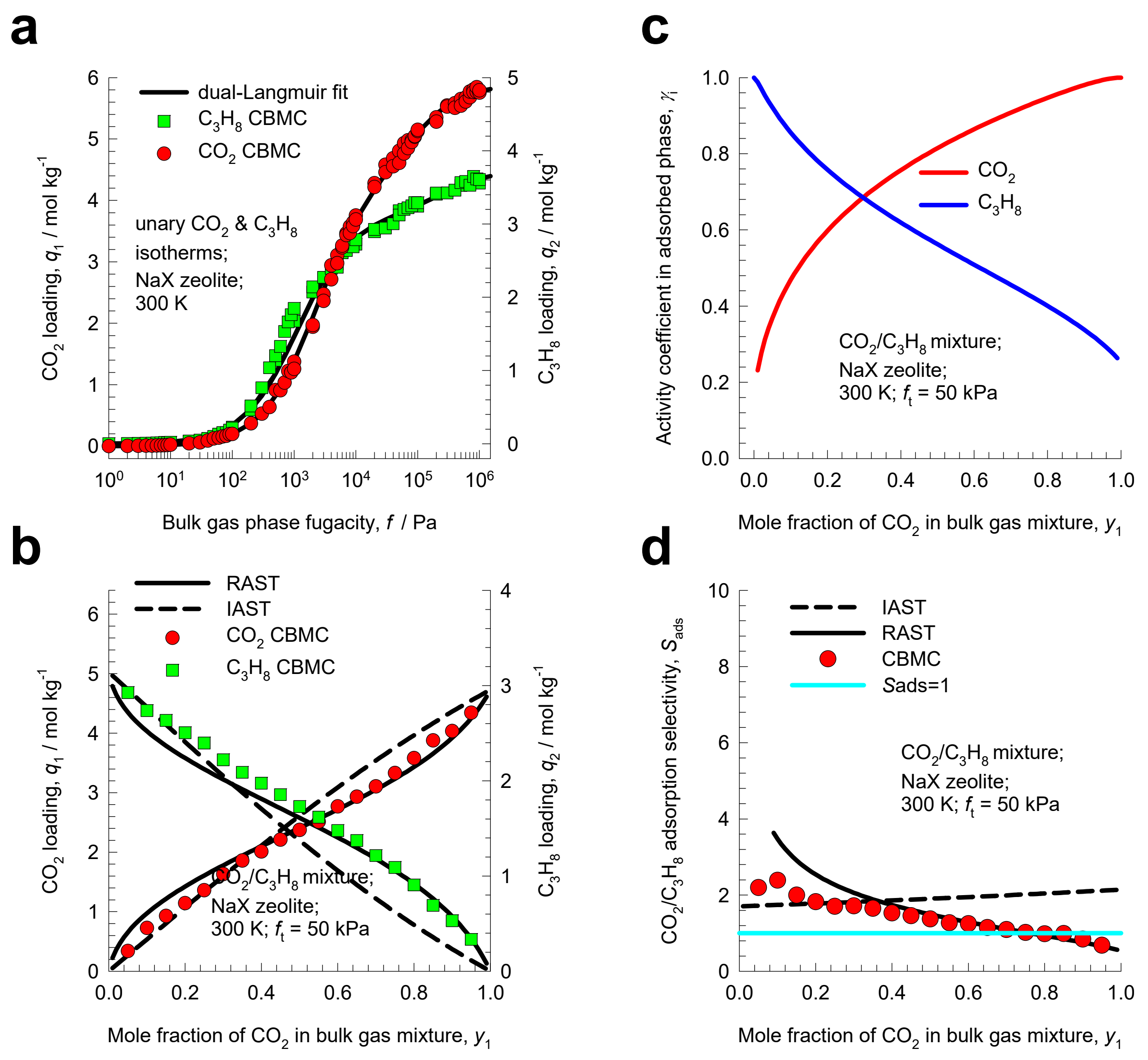

Figure S25. (a) CBMC simulations of unary isotherm data of CO_2, and C_3H_8 in NaX (106 Si, 86 Al, 86 Na^+, Si/Al=1.23) zeolite at 300 K. The isotherm fit parameters are provided in Table S8. (b) CBMC simulation data (indicated by symbols) of for component loadings, q_i, of CO_2, and C_3H_8 for adsorption of CO_2/C_3H_8 mixtures in NaX zeolite at 300 K and total fugacity f_t = 50 kPa, as function of the mole fraction of CO_2 in the bulk gas phase, y_1. (c) RAST calculations of the activity coefficients in the adsorbed phase. (d) CO_2/C_3H_8 adsorption selectivity as function of the mole fraction of CO_2 in the bulk gas phase. The dashed lines in (b), and (d) are the IAST estimations. The continuous solid lines in (b), and (d) are the estimations using RAST using fitted Wilson parameters are provided in Table S8.

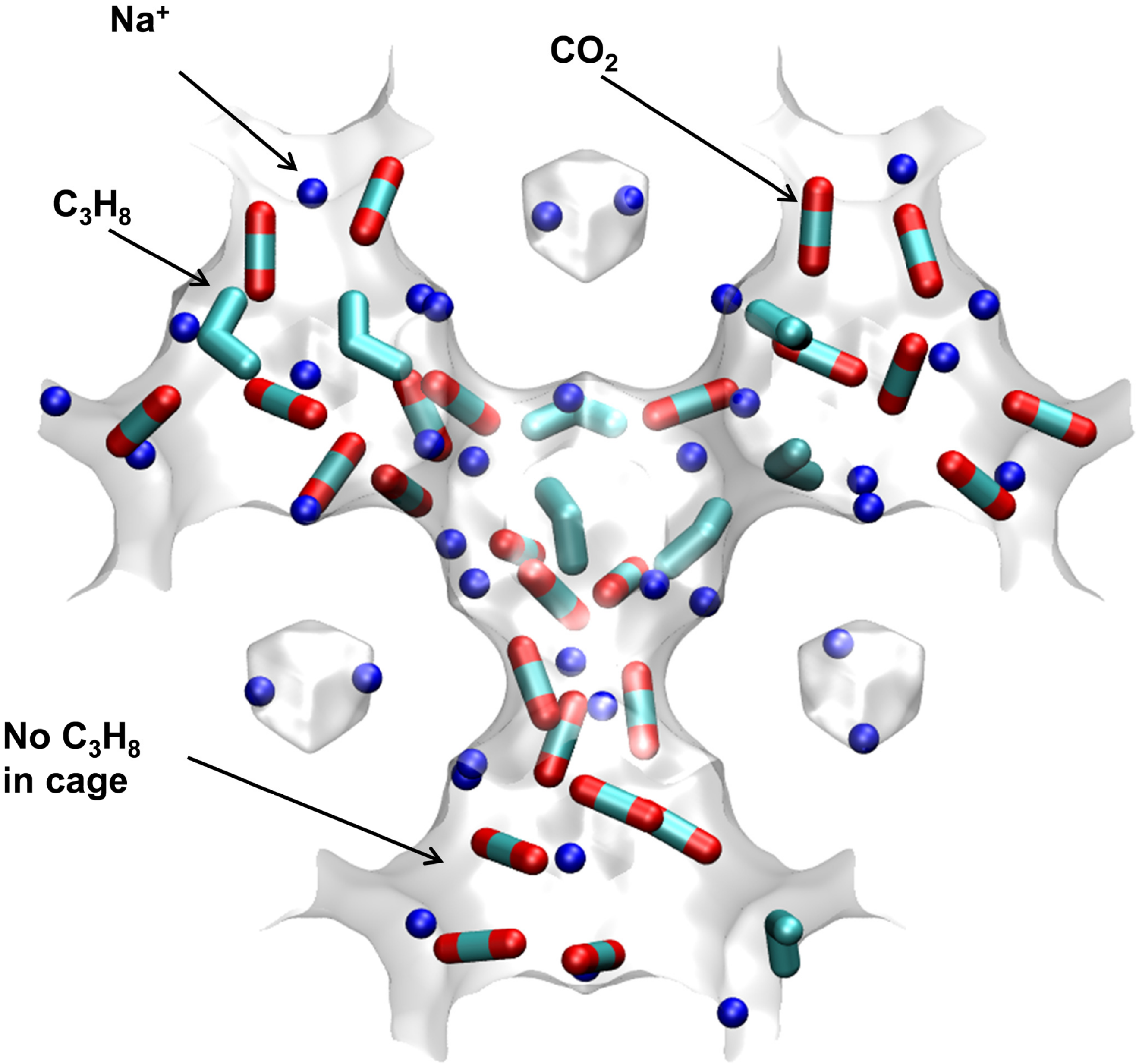

Figure S26. Computational snapshots showing the location of CO_2, and C_3H_8 within the cages of NaX zeolite at 300 K and total fugacity $f_t = 1$ MPa. The component partial fugacities are $f_1 = 0.5$ MPa, and $f_2 = 0.5$ MPa.

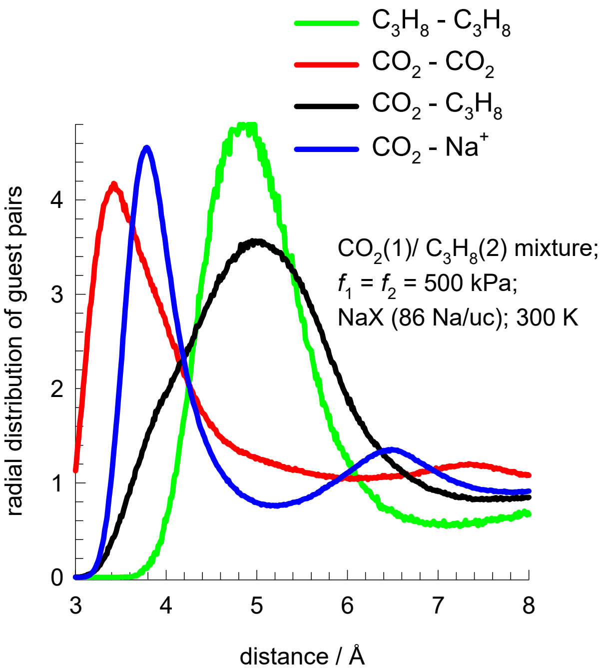

Figure S27. Radial distribution of guest pairs determined from CBMC simulations for adsorption of CO_2/C_3H_8 mixtures in NaX zeolite at 300 K and total fugacity f_t = 1 MPa, and y_1=0.5.

.

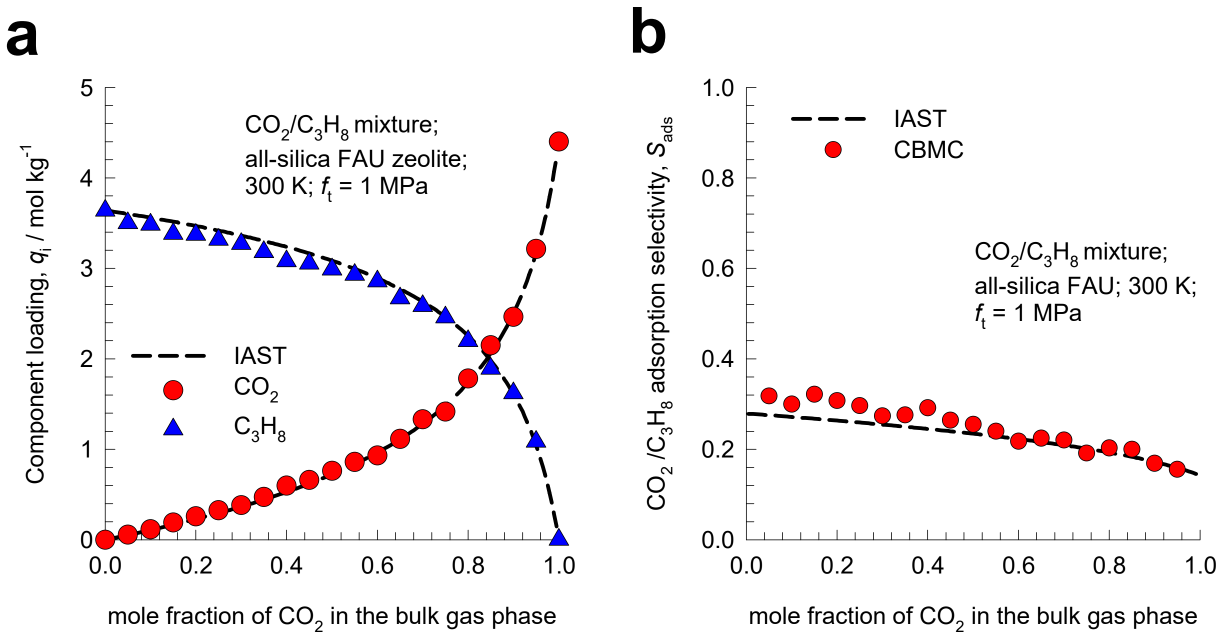

Figure S28. Comparison of CBMC simulated values of (a) component loadings, and (b) adsorption selectivities determined from CBMC simulations of CO_2/C_3H_8 mixture adsorption in all-silica FAU (192 Si, 0 Al, 0 Na^+, Si/Al=∞) zeolite at total fugacity f_t = 1 MPa and 300 K with IAST estimations. The unary isotherm parameters are provided in Table S7.

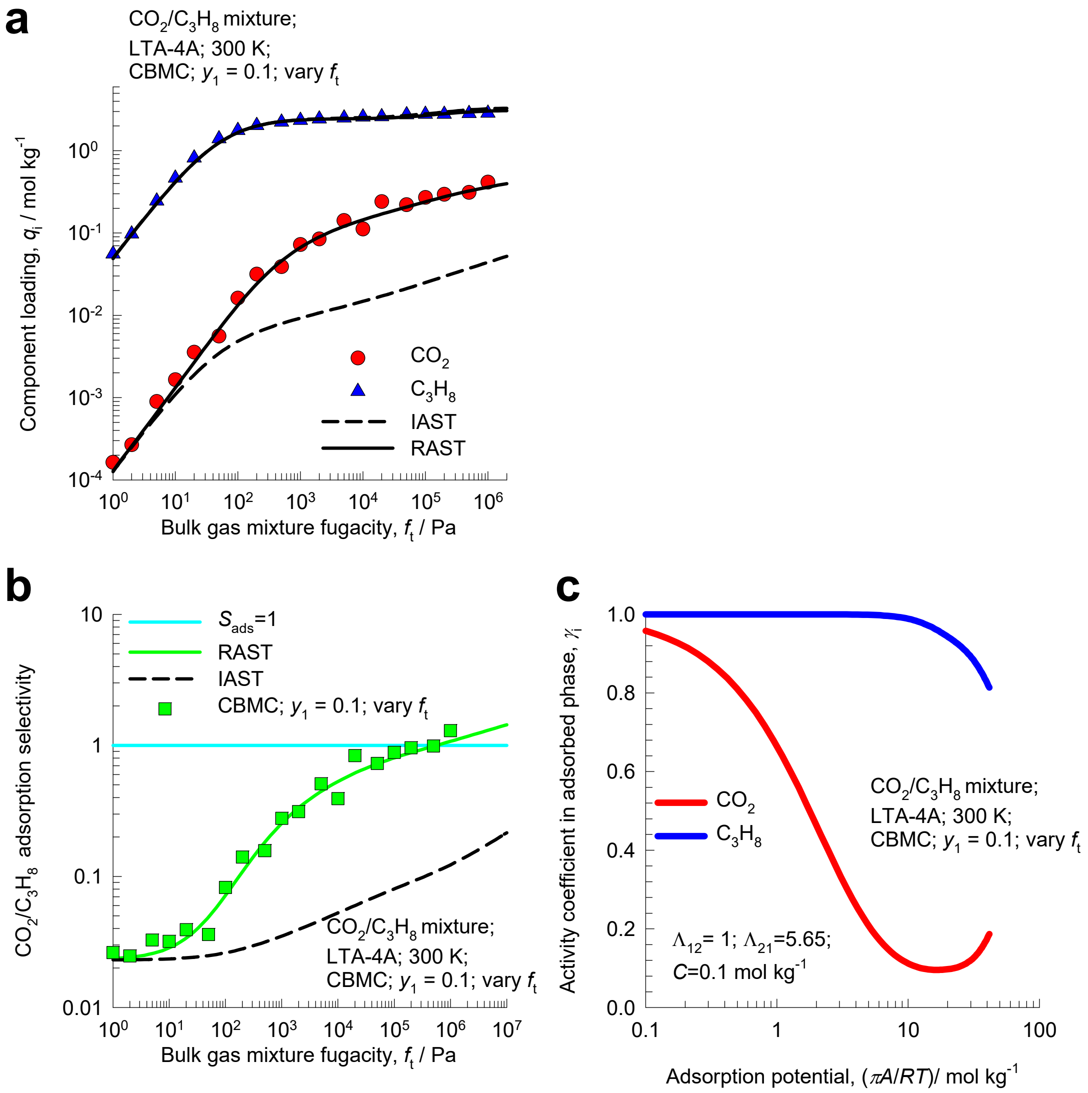

Figure S29. (a) CBMC simulations (symbols) of the component loadings for $CO_2(1)/C_3H_8(2)$ mixture adsorption in LTA-4A zeolite at 300 K, plotted as a function of the bulk gas mixture fugacity, $f_t = f_1 + f_2$; the bulk gas phase mole fractions are maintained at $y_1 = 0.1; y_2 = 0.9$. (b) The adsorption selectivity S_{ads} is plotted as a function of the bulk gas mixture fugacity, $f_t = f_1 + f_2$. The dashed lines are the IAST calculations; the continuous solid lines are RAST calculations. The unary isotherm fit parameters, along with the Wilson coefficients, are provided in Table S9. (c) RAST calculations of the activity coefficients in the adsorbed phase as function of the adsorption potential $\pi A/RT$.

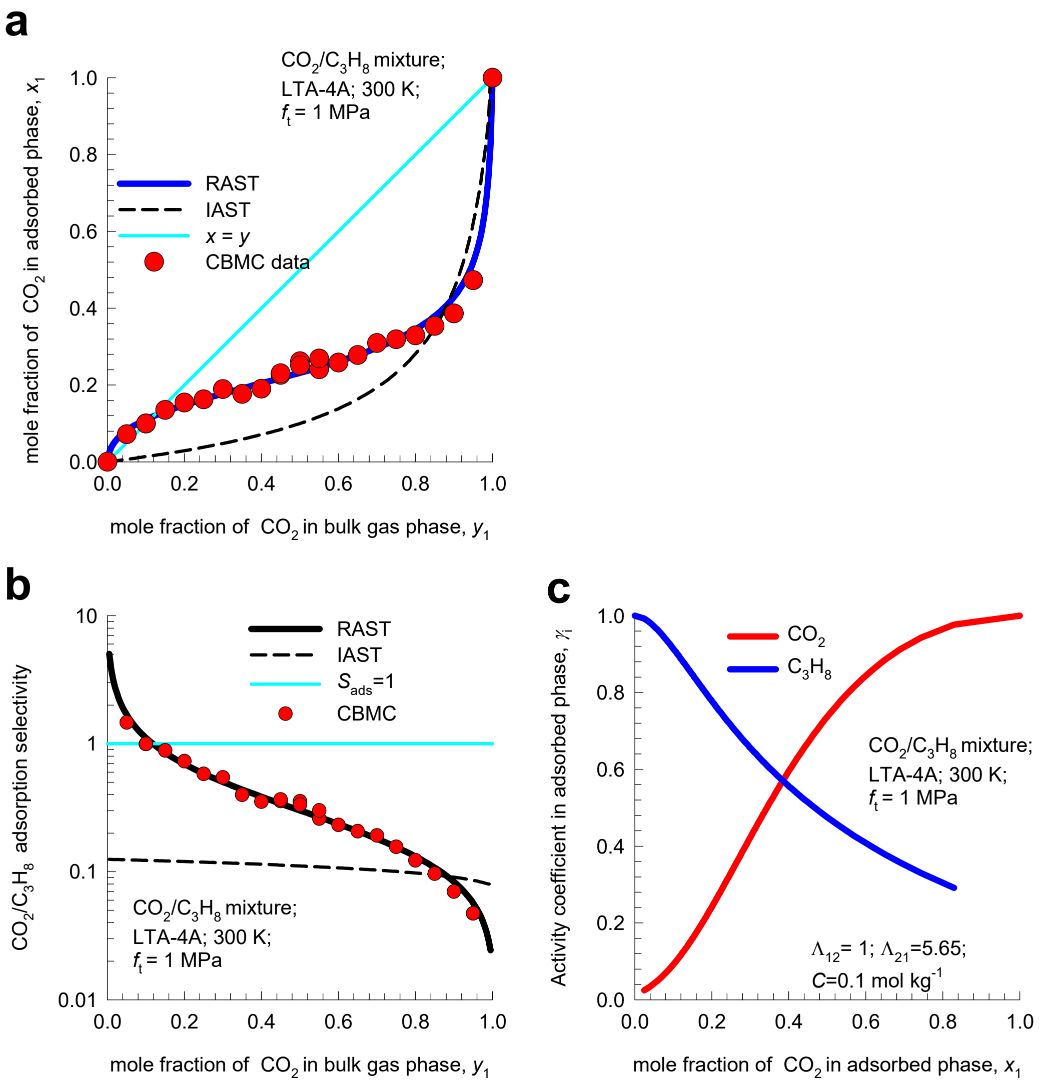

Figure S30. (a) CBMC simulation data (symbols) for $CO_2(1)/C_3H_8(2)$ mixture adsorption in LTA-4A zeolite at 300 K and total fugacity $f_t = 1$ MPa; the adsorbed phase mole fraction of $CO_2(1)$ is plotted as function of the mole fraction of CO_2 in the bulk gas phase, y_1. (b) The adsorption selectivity S_{ads} is plotted as a function of the mole fraction of CO_2 in the bulk gas phase, y_1. The dashed lines are the IAST calculations; the continuous solid lines are RAST calculations. The unary isotherm fit parameters, along with the Wilson coefficients, are provided in Table S9. (c) RAST calculations of the activity coefficients in the adsorbed phase as function of the mole fraction of CO_2 in the adsorbed phase, x_1.

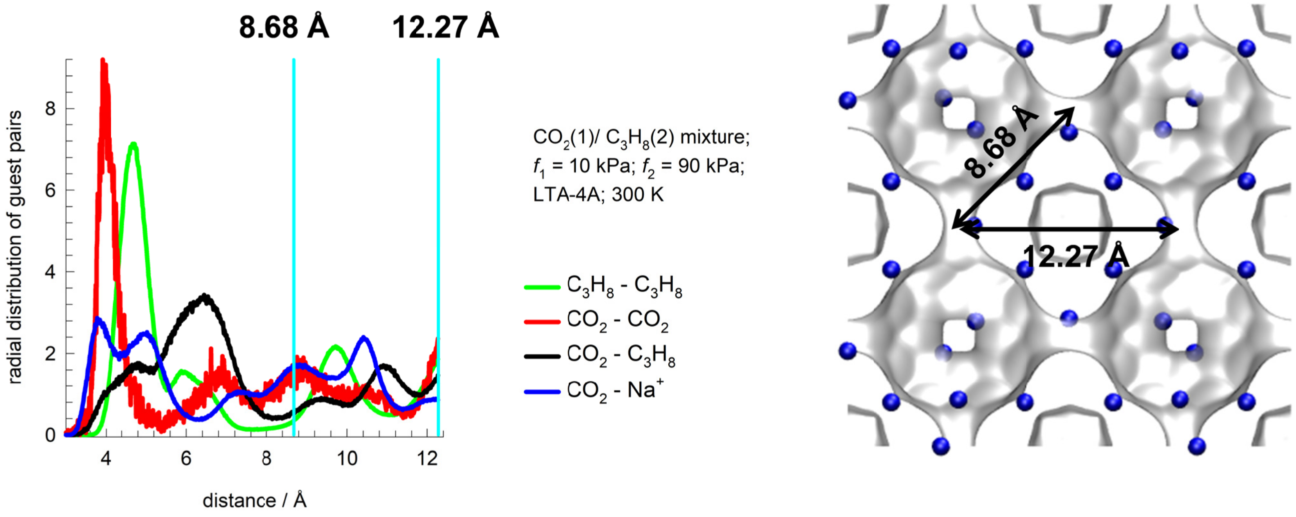

Figure S31. Radial distribution of guest pairs determined from CBMC simulations for adsorption of CO_2/C_3H_8 mixtures in LTA-4A zeolite at 300 K and total fugacity f_t = 100 kPa, and y_1=0.1.

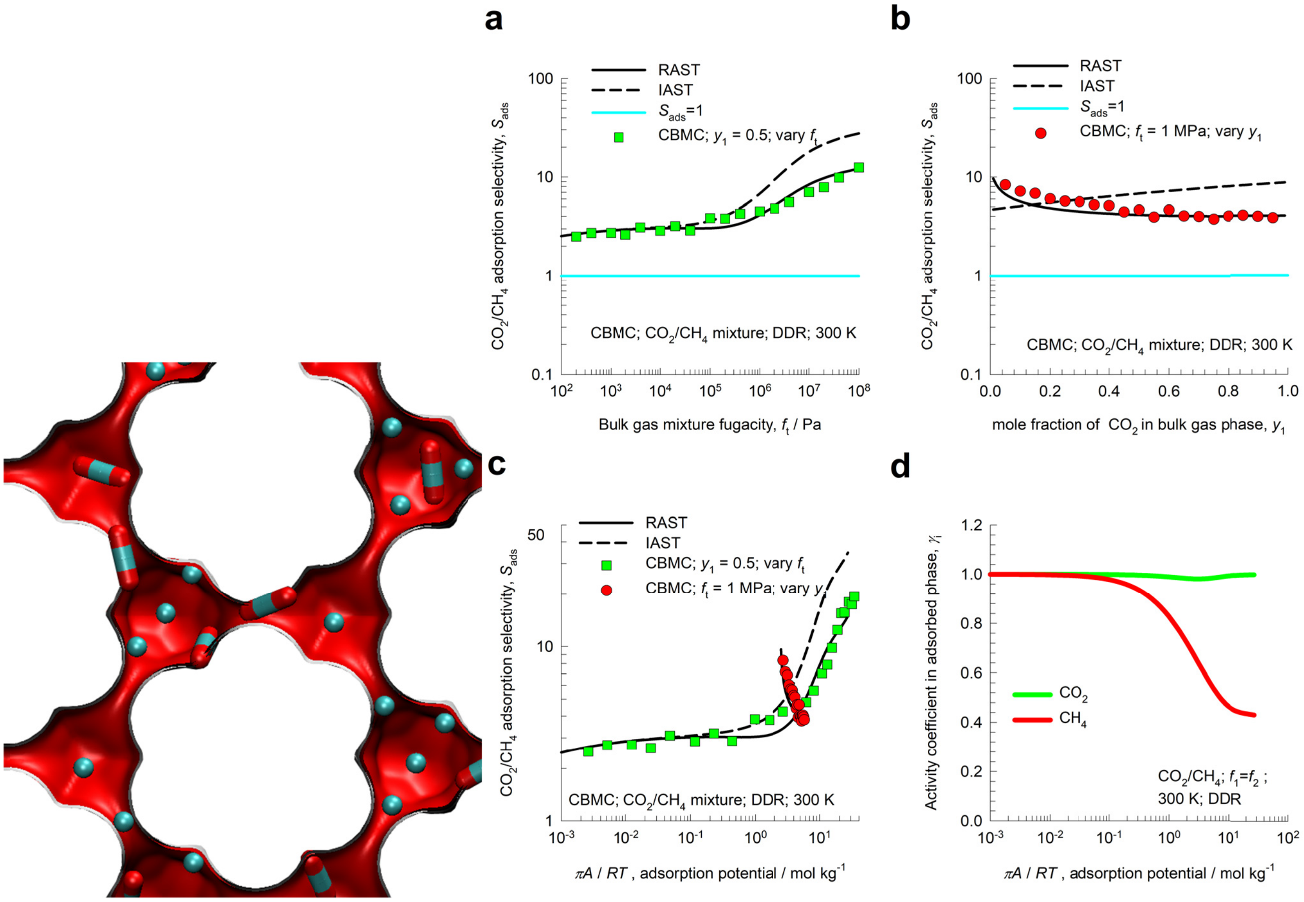

Figure S32. (a, b, c) CBMC simulations of the adsorption selectivity, S_{ads}, for CO$_2$(1)/CH$_4$(2) mixtures in DDR zeolite at 300 K. In (a) the bulk gas phase mole fractions are maintained at $y_1 = y_2 = 0.5$, and S_{ads} is plotted as a function of the bulk gas mixture fugacity, $f_t = f_1 + f_2$. In (b) the total bulk gas mixture fugacity is held constant, $f_t = f_1 + f_2 = 10^6$ Pa, and S_{ads} is plotted as a function of the bulk gas mole fraction of CO$_2$(1), y_1. In (c) both sets of data are plotted as function of the adsorption potential $\pi A/RT$. The dashed lines are the IAST calculations; the continuous solid lines are RAST calculations. The unary isotherm fit parameters and Wilson coefficients are provided in Table S10. (d) Activity coefficients in the adsorbed phase as a function of $\pi A/RT$.

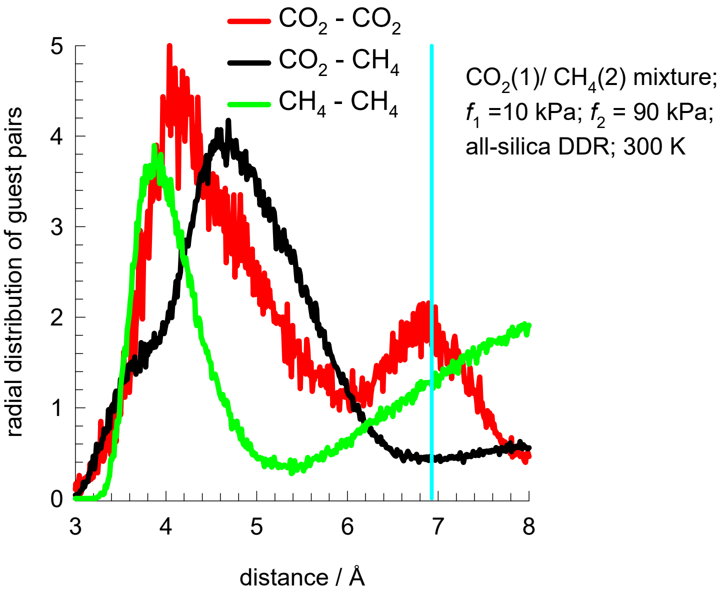

Figure S33. Radial distribution of guest pairs determined from CBMC simulations for adsorption of CO_2/CH_4 mixtures in all-silica DDR zeolite at 300 K and total fugacity f_t = 100 kPa, and y_1=0.1.

6 Nomenclature

Latin alphabet

A	surface area per kg of framework, $\mathrm{m^2\ kg^{-1}}$
b_i	Langmuir parameter, Pa^{-1}
C	constant used in Equation (S13), $\mathrm{kg\ mol^{-1}}$
f_i	partial fugacity of species *i*, Pa
f_t	total fugacity of bulk fluid mixture, Pa
G^{excess}	excess Gibbs free energy, $\mathrm{J\ mol^{-1}}$
n	number of species in the mixture, dimensionless
p_i	partial pressure of species *i*, Pa
p_t	total system pressure, Pa
P_i^0	sorption pressure, Pa
q_i	molar loading of species *i*, $\mathrm{mol\ kg^{-1}}$
q_t	total molar loading of mixture, $\mathrm{mol\ kg^{-1}}$
$q_\mathrm{i,sat}$	molar loading of species *i* at saturation, $\mathrm{mol\ kg^{-1}}$
R	gas constant, 8.314 $\mathrm{J\ mol^{-1}\ K^{-1}}$
S_ads	adsorption selectivity, dimensionless
T	absolute temperature, K
V_p	pore volume, $\mathrm{m^3\ kg^{-1}}$
x_i	mole fraction of species *i* in adsorbed phase, dimensionless
y_i	mole fraction of species *i* in bulk fluid mixture, dimensionless

Nomenclature

Greek letters

γ_i	activity coefficient of component *i* in adsorbed phase, dimensionless
Λ_{ij}	Wilson parameters, dimensionless
μ_i	molar chemical potential, J mol^{-1}
ν	Freundlich exponent, dimensionless
π	spreading pressure, N m^{-1}
ρ	framework density, kg m^{-3}

Subscripts

i,j	components in mixture
i	referring to component *i*
t	referring to total mixture
sat	referring to saturation conditions

Superscripts

0	referring to pure component loading
excess	referring to excess parameter

7 References

(1) Krishna, R.; van Baten, J. M. In silico screening of metal-organic frameworks in separation applications. *Phys. Chem. Chem. Phys.* **2011**, *13*, 10593-10616.

(2) Krishna, R.; van Baten, J. M. In Silico Screening of Zeolite Membranes for CO_2 Capture. *J. Membr. Sci.* **2010**, *360*, 323-333.

(3) Krishna, R.; van Baten, J. M. Describing Mixture Diffusion in Microporous Materials under Conditions of Pore Saturation. *J. Phys. Chem. C* **2010**, *114*, 11557-11563.

(4) Krishna, R.; van Baten, J. M. Diffusion of alkane mixtures in zeolites. Validating the Maxwell-Stefan formulation using MD simulations. *J. Phys. Chem. B* **2005**, *109*, 6386-6396.

(5) Krishna, R.; van Baten, J. M. Insights into diffusion of gases in zeolites gained from molecular dynamics simulations. *Microporous Mesoporous Mater.* **2008**, *109*, 91-108.

(6) Krishna, R. Describing the Diffusion of Guest Molecules inside Porous Structures. *J. Phys. Chem. C* **2009**, *113*, 19756-19781.

(7) Krishna, R. Diffusion in Porous Crystalline Materials. *Chem. Soc. Rev.* **2012**, *41*, 3099-3118.

(8) Ryckaert, J. P.; Bellemans, A. Molecular dynamics of liquid alkanes. *Faraday Discuss. Chem. Soc.* **1978**, *66*, 95-106.

(9) Dubbeldam, D.; Calero, S.; Vlugt, T. J. H.; Krishna, R.; Maesen, T. L. M.; Smit, B. United Atom Forcefield for Alkanes in Nanoporous Materials. *J. Phys. Chem. B* **2004**, *108*, 12301-12313.

(10) García-Pérez, E.; Parra, J. B.; Ania, C. O.; García-Sánchez, A.; Van Baten, J. M.; Krishna, R.; Dubbeldam, D.; Calero, S. A computational study of CO_2, N_2 and CH_4 adsorption in zeolites. *Adsorption* **2007**, *13*, 469-476.

(11) García-Sánchez, A.; Ania, C. O.; Parra, J. B.; Dubbeldam, D.; Vlugt, T. J. H.; Krishna, R.; Calero, S. Development of a Transferable Force Field for Carbon Dioxide Adsorption in Zeolites. *J. Phys. Chem. C* **2009**, *113*, 8814-8820.

(12) Ruthven, D. M. *Principles of Adsorption and Adsorption Processes*. John Wiley: New York, 1984.

(13) Myers, A. L.; Prausnitz, J. M. Thermodynamics of Mixed Gas Adsorption. *A.I.Ch.E.J.* **1965**, *11*, 121-130.

(14) Siperstein, F. R.; Myers, A. L. Mixed-Gas Adsorption. *A.I.Ch.E.J.* **2001**, *47*, 1141-1159.

(15) Talu, O.; Myers, A. L. Rigorous Thermodynamic Treatment of Gas-Adsorption. *A.I.Ch.E.J.* **1988**, *34*, 1887-1893.

(16) Talu, O.; Zwiebel, I. Multicomponent Adsorption Equilibria of Nonideal Mixtures. *A.I.Ch.E.J.* **1986**, *32*, 1263-1276.

(17) Gholipour, F.; Mofarahi, M. Adsorption Equilibrium of Methane and Carbon Dioxide on Zeolite13X: Experimental and Thermodynamic Modeling. *J. of Supercritical Fluids* **2016**, *111*, 47-54.

(18) Mofarahi, M.; Gholipour, F. Gas Adsorption Separation of CO_2/CH_4 System using Zeolite 5A. *Microporous Mesoporous Mater.* **2014**, *200*, 47-54.

(19) Hefti, M.; Marx, D.; Joss, L.; Mazzotti, M. Adsorption Equilibrium of Binary Mixtures of Carbon Dioxide and Nitrogen on Zeolites ZSM-5 and 13X. *Microporous Mesoporous Mater.* **2015**, *215*, 215-228.

References

(20) Wilkins, N. S.; Rajendran, A. Measurement of competitive CO_2 and N_2 adsorption on Zeolite 13X for post-combustion CO_2 capture. *Adsorption* **2019**, *25*, 115-133. https://doi.org/10.1007/s10450-018-00004-2.

(21) Costa, E.; Calleja, G.; Jimenez, A.; Pau, J. Adsorption Equilibrium of Ethylene, Propane, Propylene, Carbon Dioxide, and Their Mixtures in 13X Zeolite. *J. Chem. Eng. Data* **1991**, *36*, 218-224.

(22) Krishna, R.; van Baten, J. M. Segregation effects in adsorption of CO_2 containing mixtures and their consequences for separation selectivities in cage-type zeolites. *Sep. Purif. Technol.* **2008**, *61*, 414-423.

(23) Krishna, R.; van Baten, J. M.; Baur, R. Highlighting the Origins and Consequences of Thermodynamic Nonidealities in Mixture Separations using Zeolites and Metal-Organic Frameworks. *Microporous Mesoporous Mater.* **2018**, *267*, 274-292. http://dx.doi.org/10.1016/j.micromeso.2018.03.013.

(24) Krishna, R.; van Baten, J. M. Investigating cluster formation in adsorption of CO_2, CH_4, and Ar in zeolites and metal organic frameworks at sub-critical temperatures. *Langmuir* **2010**, *26*, 3981-3992.

(25) Krishna, R.; van Baten, J. M. Highlighting a variety of unusual characteristics of adsorption and diffusion in microporous materials induced by clustering of guest molecules. *Langmuir* **2010**, *26*, 8450-8463.